Escola de Camins
Escola Tècnica Superior d'Enginyeria de Camins, Canals i Ports
UPC BARCELONATECH

Tile Vaults as Integrated Formwork for Concrete Shells: Study of the Influence of the Model Network in the Reinforcement Design

TREBALL FINAL DE MÀSTER

Treball realitzat per:

Yuanpeng Liu

Dirigit per:

Prof. Dr. Pere Roca

Dr. David López López

Màster en:

Enginyeria de Camins, Canals i Ports

Barcelona, 25/01/2021

Departament d'Enginyeria Civil i Ambiental (DECA)

AKNOWLEDGEMENTS

First of all, I would like to express my gratitude to The Polytechnic University of Catalonia (UPC) and Tongji University for providing me this opportunity to have such a wonderful experience in my life.

I would like to thank my supervisors, Prof. Pere Roca and Dr. David López López, for their instructions and support throughout the whole research. We had a lot of discussions, and each time, they can help me solve my puzzles, offer me constructive feedback, and light my way to proceed. Without whom, this work cannot be finished.

I am indebted to Prof. Lu from Tongji University for his help and support during my master's period. He shared with me not only academic knowledge but also life experiences. His encouragement provided me the courage to pursue my dreams and to do what I like.

Thanks to my friends in Barcelona, with whom I had fascinating talks. I will always remember you together with this beautiful city.

Special thanks to Xin for always being with me and behind me.

Last but not least, I would like to thank my family for their permanent care, love, encouragement, and support.

ABSTRACT

Extended Limit Analysis for Reinforced Masonry (ELARM) is a method that allows to design and analyze two- or three-dimensional reinforced concrete, masonry, and composite shells of most shapes. For the design of reinforced concrete shells by ELARM, random choices of parameters and the form diagram may lead to conservative results, i.e., a considerable amount of reinforcement. This research aims to find out how to choose proper parameters and the form diagram to reduce reinforcement usage.

In this dissertation, an algorithm is proposed to search for the optimal values of the steel bar direction, the reinforcement position, and the thrust network height to determine the least reinforcement amount for a given form diagram. Besides, a series of form diagrams for vaults of different geometries under various load cases are tested to investigate the influence of the form diagram's pattern on the reinforcement amount. The results reveal that, apart from the form diagram's pattern, other two factors, the force distribution in the form diagram and the process to calculate the assigned width in ELARM3D, may also affect the reinforcement amount and need further research. Besides, based on the results, some recommendations are provided for the users of ELARM3D of the current version on how to build a proper form diagram, which requires a relatively low amount of reinforcement.

RESUMEN

El análisis límite extendido al caso de la mampostería reforzada (ELARM) es un método que permite diseñar y analizar hormigón armado, mampostería y láminas s compuestas bidimensionales o tridimensionales con una variedad de formas. Para el diseño de láminas de hormigón armado por ELARM, la elección aleatoria de parámetros y el diagrama de forma pueden conducir a resultados conservadores, es decir, una cantidad considerable de refuerzo. Esta investigación tiene como objetivo investigar cómo elegir los parámetros adecuados y el diagrama de forma para reducir el uso de refuerzos.

En esta disertación, se propone un algoritmo para buscar los valores óptimos de la dirección de las barras de acero, la posición del refuerzo y la altura de la red de empuje para determinar la cantidad mínima de refuerzo para un diagrama de forma dado. Además, se ensayan una serie de diagramas de forma para bóvedas de diferentes geometrías bajo varios casos de carga para investigar la influencia del patrón del diagrama de forma en la cantidad de refuerzo. Los resultados revelan que, además del patrón del diagrama de forma, otros dos factores, la distribución de fuerza en el diagrama de forma y el proceso para calcular el ancho asignado en ELARM3D, también pueden afectar la cantidad de refuerzo y necesitan más investigación. Además, con base en los resultados, se proponen algunas recomendaciones para los usuarios de ELARM3D en su versión actual sobre cómo construir un diagrama de forma adecuado, lo que requiere una cantidad relativamente baja de refuerzo.

LIST OF CONTENTS

LIST OF FIGURES

LIST OF TABLES

1. INTRODUCTION

1.1. Introduction

Tile vaults (also called thin-tile, timbrel, Catalan, or Guastavino vaults) are unreinforced masonry structures made of thin bricks (tiles), mortar, and fast-setting cement or gypsum. Bricks can be built up to two, three, or more layers. For the first layer, thanks to the light weight of bricks and the quick adhesion of fast-setting cement or gypsum, it can be built without the need for centering or formwork except at the boundaries. The upper layers can then be built based on the first layer, which works as a stay-in-place formwork. Inspired by this inherently economic characteristic of tile vaults, a new construction method for curved and spatial concrete shells has been developed recently [1]. Using tile vaults as integrated formwork for reinforced concrete shells significantly reduces the construction costs by avoiding additional formwork, which is typically expensive. For details of the construction system, readers are referred to reference [1].

The combination of masonry and reinforced concrete creates a new type of composite structure that requires new numerical methods to conduct the analysis. ELARM3D, which is a method developed by López López [2], allows the design and analysis of spatial composite shells based on thrust network analysis (TNA) [3] and limit analysis [4]. ELARM3D applies limit analysis, which is commonly used for the analysis of masonry arches, but using a thrust network rather than a thrust line to consider for three-dimensional structures and virtual boundaries instead of real boundaries of the vault to indirectly take into account the additional tensile and bending strength provided by the steel reinforcement. In ELARM3D, the thrust network is generated using TNA based on two planar diagrams, the form diagram, and the force diagram. The form diagram describes the force paths through which the structure's self-weight and external forces are transferred to the supports. The force diagram represents the magnitude of the horizontal component of the resultant forces in the force paths.

1.2. Problem statement

When applying ELARM3D to design a new reinforced concrete shell, it is observed that with different assumptions of force paths, i.e., form diagrams, the required amount of reinforcement may vary significantly. Even for a fixed form diagram, some other parameters, for example, the direction and position of the steel bars, may also influence the required reinforcement amount remarkably. For the users of ELARM3D, there is currently no guideline for them on how to choose a proper form diagram and appropriate values of related parameters such that the required reinforcement amount can reach a low level. Random choices of the form diagram and the related parameters would lead to conservative results, thus, waste of materials. As the global warming issue is increasingly pressing, it is essential to save materials from the design phase.

Therefore, based on the above discussions, two main problems can be distilled:

1. How to define the related parameters in ELARM3D such that the required reinforcement amount reaches a low level for a given form diagram.
2. How to define the form diagram in ELARM3D so that the required reinforcement amount is at a low level for shells of different geometries under various load cases.

1.3. Research objectives

An algorithm is proposed in this dissertation to find the best set of parameters such that the necessary reinforcement amount can reach the minimum for a given form diagram.
To investigate the influence of the form diagram's pattern on the necessary reinforcement amount, this research explores a series of form diagrams for shells of different geometries under various load cases. Based on the numerical results, some recommendations can be summarized for the users of ELARM3D on how to build a proper form diagram that requires low reinforcement amount.

1.4. Outline of chapters

This dissertation presents a literature review of related aspects in chapter 2, proposes an algorithm to search for the best set of parameters to determine the least amount of reinforcement for a given form diagram in chapter 3, and tested a series of form diagrams for several different shells under multiple load cases in chapter 4. Detailed discussions and analysis regarding the obtained numerical results are provided in chapter 5. The conclusions and some recommendations for selecting the proper form diagram are listed in chapter 6, together with possible future works.

2. LITERATURE REVIEW

2.1. Graphic statics

The statical analysis may be carried out either numerically or graphically. The graphical method is called graphic statics. The origin of graphic statics can be traced back to Simon Stevin who was the first person to represent a force as a vector and also presented a correct interpretation of the parallelogram of forces which is a graphical method for solving the results of applying two forces to an object [5]. This was the start of equilibrium analysis of structural systems, and also the start of graphical methods. Then, Karl Culmann was the first to formalize graphical analysis as a powerful method for equilibrium analysis in structural engineering [6]. He is generally acknowledged as the father of graphic statics. In his book *Die graphische Statik* [7], he presented the first consistent comprehensive body of graphical techniques and introduced many fundamental and useful skills which can be applied to a wide variety of structural problems.

According to reference [8], "*the creation of a force diagram from a form diagram (with its external applied forces) is called Graphic Statics*". Indeed, when applying graphic statics, two diagrams are needed. One is the form diagram (funicular polygon) and the other one is its corresponding force diagram (force polygon). These two diagrams are reciprocal figures that they are geometrically related such that corresponding branches are parallel and branches which come together in a node in one of the networks form a closed polygon in the other and vice versa [9]. The form diagram provides the length and the angle of each member, and the length of each branch in the force diagram is proportional to the force in the corresponding member.

Fig. 1 is used to illustrate the basic idea of applying graphic statics to solve a simple problem. On the right is the funicular polygon, where the connectivity, geometry, and boundary conditions are shown for a rope under five external point loads. Once its corresponding force polygon is constructed through graphic statics (Fig. 1, left), the axial forces in the rope can be determined through measuring the lengths of the branches in the force polygon. The five triangles in the middle are separate force polygons which also represent the equilibrium of forces at each node in the form diagram. For detailed tutorials of how to construct these two diagrams and practical applications of graphic statics, one can refer to the book of Edward Allen and Waclaw Zalewski [10].

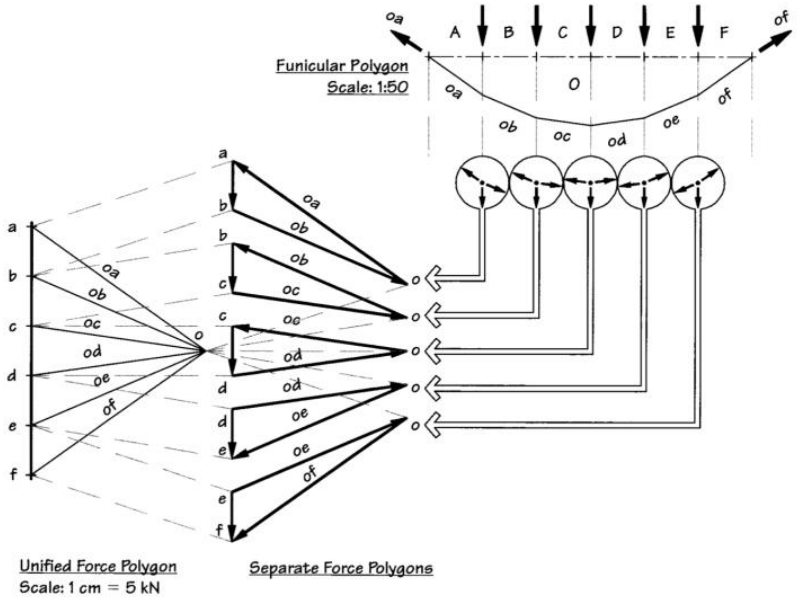

Fig. 1. Funicular polygon and force polygon [10], and the notation here follows Bow's rules [11]

Graphic statics was successfully used in engineering practice in history, for example, the design of the Eiffel Tower, the design of Sagrada Família, the study of Mallorca Cathedral, etc. (Fig. 2). However, by 1920, graphical methods were largely replaced by the theory of elasticity which provides precise closed-form analytical solutions and doesn't require tedious drawings. Now due to the advent of computer-aided drawing, the process of drawing was largely eased and, as a result, graphical statics is starting to attract more and more modern scholars, engineers, and architects [6, 12-13].

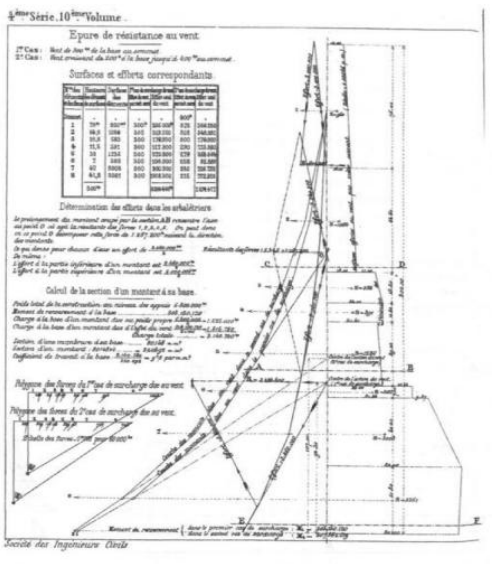

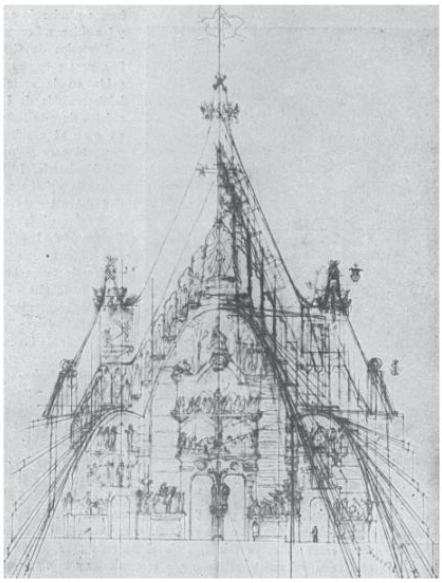

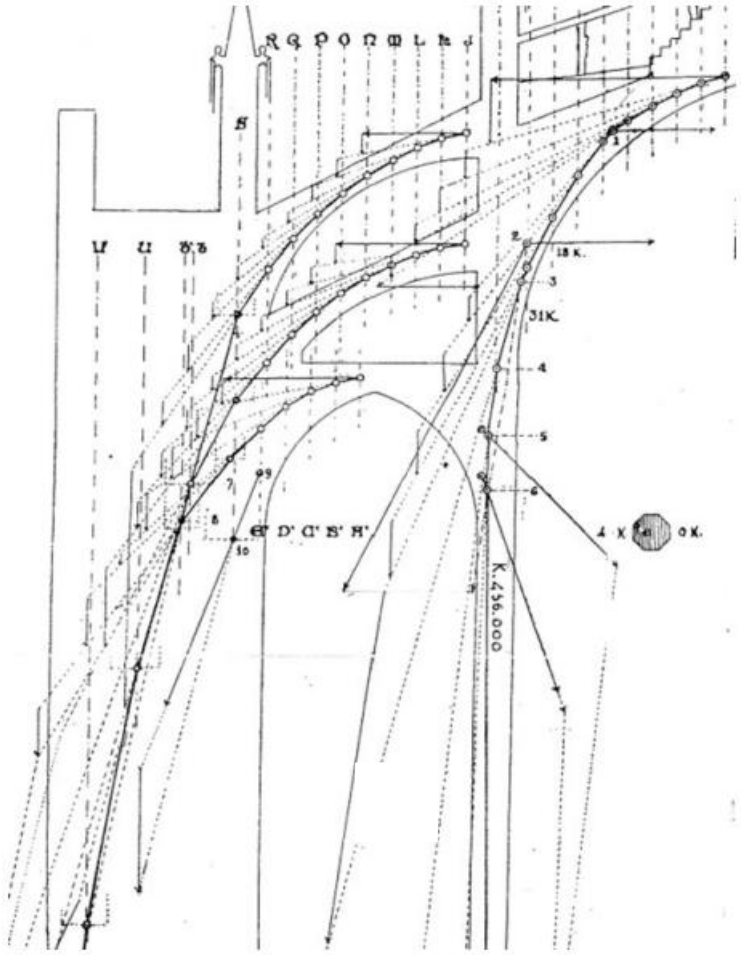

Fig. 2. Top left, a drawing of using graphic statics to design the Eiffel Tower [10];
Top right, a drawing of using graphic statics to design the Sagrada Família [14];
Bottom, Rubió's application of graphic statics to analyze the stability of Mallorca Cathedral [15]

2.2. Safe theorem

There were already some theories of masonry applied to design and analyze masonry structures in history. However, it was Heyman in his milestone paper [4] who first exposed and discussed in a rigorous and general way the application of the theory of limit analysis, which was originally developed for steel frames, to masonry structures.

To apply the theory of plasticity to masonry structures, the material should fulfill three conditions: (1) the material has an infinite compressive strength, (2) the material has null tensile strength, and (3) there is no sliding between the blocks. The first condition seems to be unsafe. However, for most historical masonry structures built with traditional techniques and geometries, considering the fact that the stress levels in these structures are only one or two order of magnitude below the crushing capacity of the stone [14] (according to local experience in Barcelona, the stress levels in masonry structures may reach the same order of magnitude but still below the crushing capacity of the stone), this one is acceptable. Stress concentrations can arise which will lead to distress

evidenced by splitting or surface spalling, while such distress is local, and normally will not lead to overall failure or buckling [16]. For the design of a new shell, before applying limit analysis to verify its stability, one must check the stresses in the material to ensure that they are lower than the compressive strength. The second condition is safe, due to the inherent tensile strength of masonry and the low adherence of mortar between blocks. The third condition is related to the high friction coefficients of masonry and is based on many observations and a large experience. Occasionally, particular precautions must be taken to avoid slip, for example, the pinnacle being an effective compressive prestressing agent to prevent sliding failure for a buttressing pier, but in general, it is rare for a masonry structure to be distressed in this way [16]. As Ochsendorf stated, "*Naturally, there are some exceptions to these assumptions, and the analyst must check their validity in each particular case"* [17]. For detailed discussions of these three conditions and some exceptions, the author refers to Heyman's treatise [16].

Accepting such postulates on the material, the safe theorem may be stated as follows, "*If a line of thrust can be found which is in equilibrium with the external loads and which lies wholly within the masonry, then the structure is safe*" [16]. Here, the thrust line is the locus of the application points of the internal forces (stress resultants) through the interfaces between the blocks, and can be found graphically using graphic statics (mentioned in section 2.1). It should be noted that in order to satisfy the safe theorem, there is no need for the line of thrust to be the "actual" one. Actually, it is difficult or even impossible to find the "actual" thrust line, or in another word, the "real" equilibrium state, as it is related to the specific details, for example, the support conditions, material properties, and cracks of a particular historic structure. Finding any line in equilibrium with the external loads and lying within the masonry is sufficient to ensure stability.

2.3. The limitations of elastic linear analysis for masonry structures

Elastic linear analysis is a common tool used to analyze steel and reinforced concrete structures. However, for masonry structures, it may not be suitable, because it does not take into account the non-tension response and other essential features of masonry behavior.

As illustrated by Block [13] in the example of Fig. 3, a finite element analysis (FEA) based on linear elastic analysis was done to two masonry arches of different thickness to radius ratios under self-weight and supported on rigid foundations. Though the FEA provides possible stress distributions in the structures, the results may be not reliable because the material is assumed to be capable to resist tension. If still trying to understand and explain the results, cracking may be predicted in the crown of the arches due to the thin compression zone on the extrados and the tension zone on the intrados. However, the results do not say anything about the stability or collapse of the arches.

In contrast, a simple limit analysis (in section 2.2), clearly reveals the key point. For the thicker arch, it is safe according to the safe theorem. However, the arch with a lower thickness to radius

ratio is too thin to contain a thrust line, because the thrust line always goes beyond the boundary of the arch as shown in the rectangles in Fig. 3. Therefore, it may not be able to stand under its self-weight.

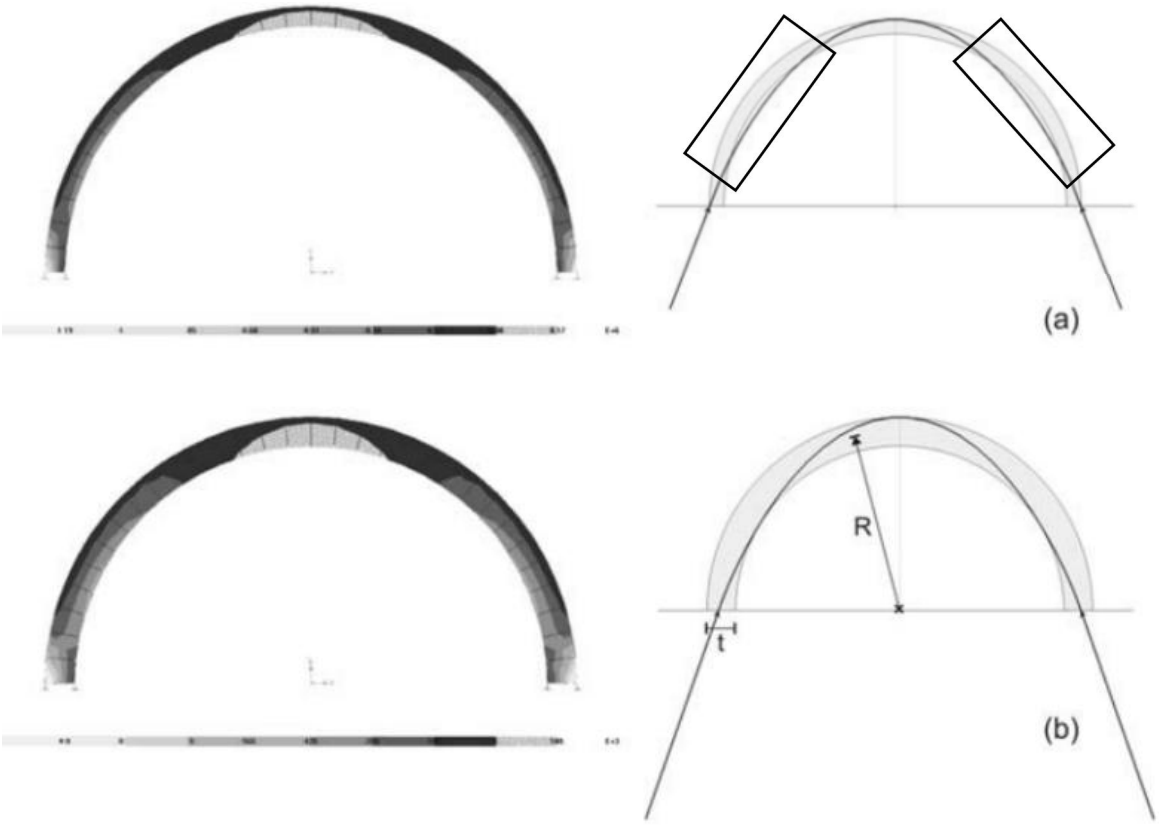

Fig. 3. Two arches of different thickness to radius ratios analyzed respectively by the finite element method based on elastic linear analysis (left) and the limit analysis (right) [13]

In short, as Roca stated, "*Attempts to use linear elastic analysis to dimension arches may result in very conservative or inaccurate approaches. Linear elastic analysis is not useful, in particular, to estimate the ultimate response of masonry structures and should not be used to conclude on their strength and structural safety*" [15].

2.4. Slicing technique

Thrust line analysis, which is based on graphic statics and Heyman's safe theorem, allows exploring possible equilibrium states in masonry structures. However, it is primarily a two-dimensional technique and is, therefore, most suitable for the analysis of arches, flying buttresses, or any structure that can be reduced to a sectional analysis. Apart from these ones, three-dimensional spatial masonry vaults can be also analyzed using thrust line analysis when combined with the slicing technique, which divides the vault into elementary arches or strips, simplifying the behavior of the vault to a combination of two-dimensional problems [18]. To make such simplifications, some scholars in history imagined that the thrust would follow the same path

as a ball rolling on the extrados (as explained in Fig. 4, left). On the right side of Fig. 4, an example of a way to slice a groin vault is provided.

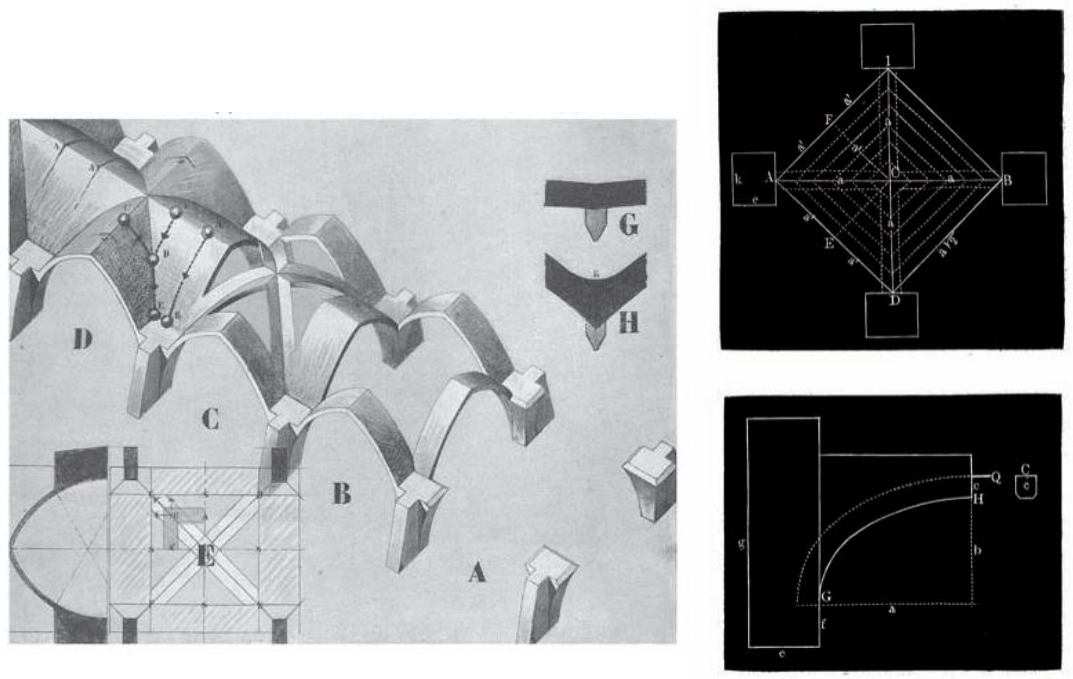

Fig. 4. Left, the assumption that thrust would follow the path as a ball rolling on the extrados (Abraham, 1934) [14];
Right, Scheffler analysis using the slicing technique (Scheffler, 1857) [14].

The slicing technique, though could be used to analyze most of historical masonry vaults, cannot capture the full three-dimensional behavior of the structure [3]. For example, Poleni analyzed the dome of St Peter's in Rome by slicing it into a series of lunes (Fig. 5, Left) [19]. However, this analysis neglects the compressive hoop stresses in the upper part of the dome and cracks would only happen in the lower part (Fig. 5, Right) [19]. Thus, the accuracy of the results would largely depend on the slicing pattern chosen by the analyst. In addition, this method can very time-consuming.

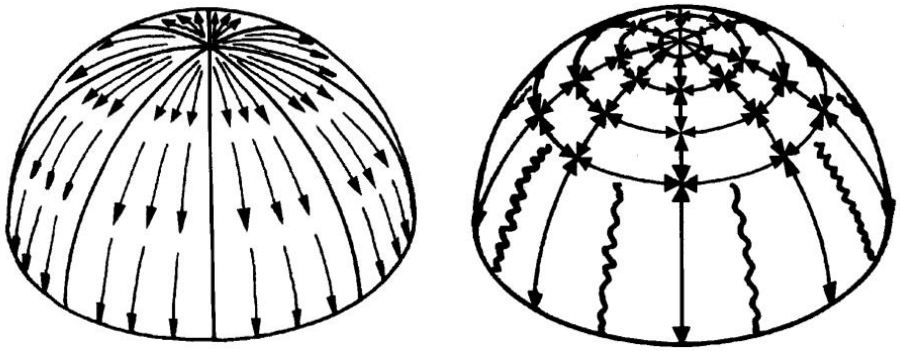

Fig. 5. Left, imagined load paths of a dome through slicing it into a series of lunes [19];
Right, the compressive hoop stresses in the upper part of the dome, and cracks happen in the lower part of the dome [19].

2.5. Force network method

With the advent of computer technology, O'Dwyer [19] proposed a promising equilibrium approach based on force networks. This method can capture the three-dimensional behavior of the structure and can be programmed to realize highly efficient calculations.

Firstly, force paths need to be assumed, and a planar mesh is constructed based on these imagined force paths. Fig. 6 shows the examples of two assumptions of force paths and a possible planar mesh for a groin vault. Then, through formulating vertical equilibrium constraints at all nodes, a series of force networks can be obtained. In the end, optimization methods have to be used to find the optimal shape of the force network which fits inside the real boundary of the structure.

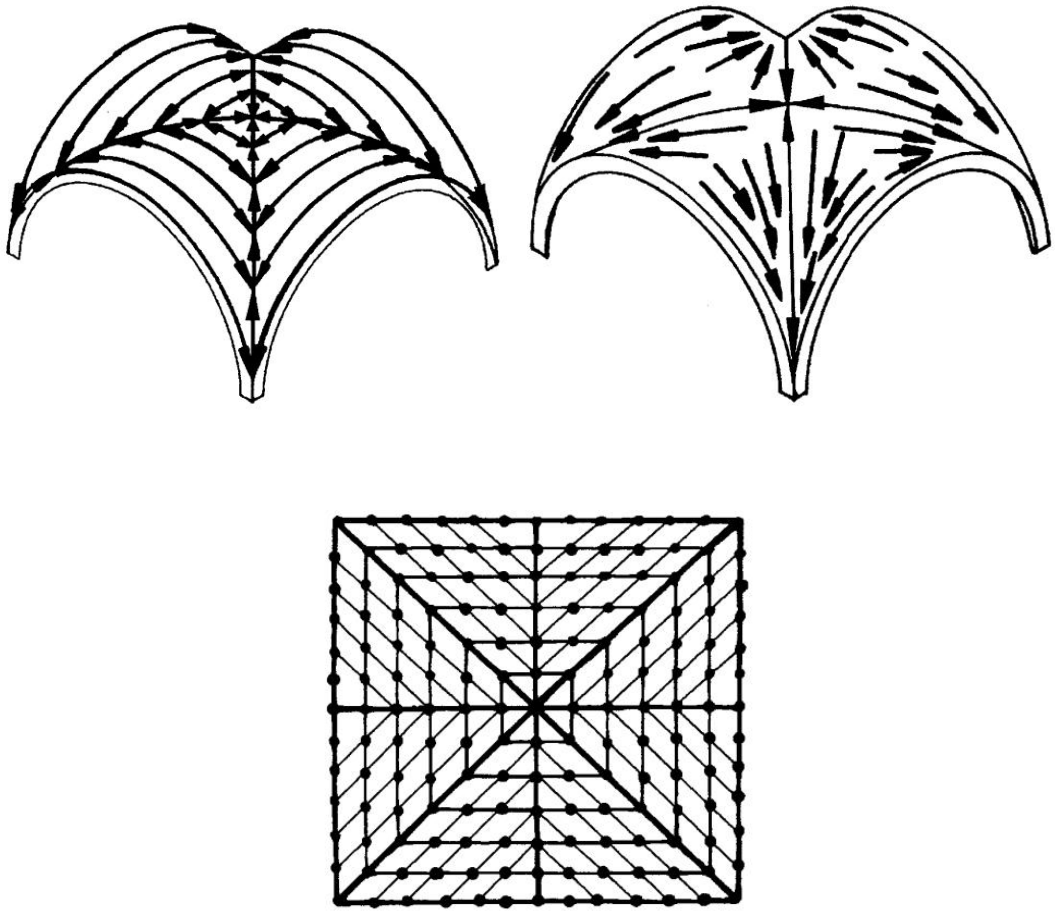

Fig. 6. Top, two assumptions of force paths in a groined vault [19];
Bottom, an assumed planar mesh of a groined vault [19].

Though this method allows exploring different assumptions of force paths through using different planar meshes, the main drawback is that it does not permit the change of force distributions. Besides, the results of this method rely largely on the chosen mesh, so that the analyst needs to be equipped with a certain level of experience and knowledge of the vault to find an appropriate one.

2.6. Thrust network analysis

2.6.1. Main steps of thrust network analysis

Based on the framework of O'Dwyer's method, Block [3] developed a new methodology which is thrust network analysis (TNA). TNA extends the force network method by incorporating graphic statics to allow control of the force distribution in the vault.

The main steps of thrust network analysis are as follows,

1. A form diagram (primal grid), which is the projection of the thrust network in the horizontal plane, should be constructed by the analyst at first. It represents the assumed force paths in the vault (Fig. 7). This is similar to the concept of the planar mesh in the force network method (section 2.5).

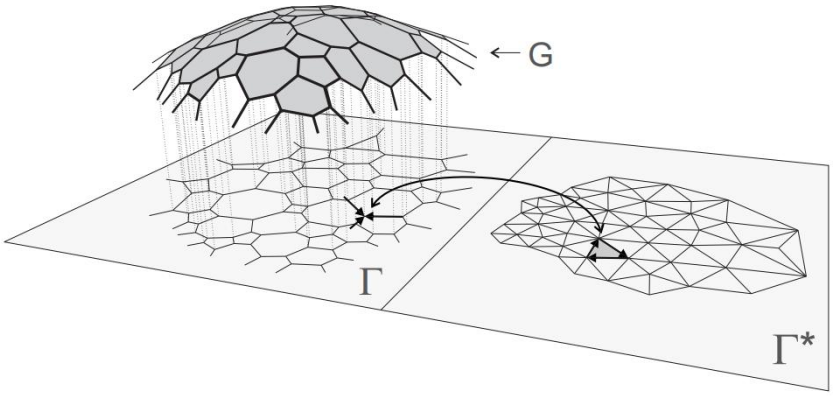

Fig. 7. Relationship between the compression equilibrium shape, the thrust network, its planar projection (form diagram), and the reciprocal diagram (force diagram) [3]

2. A force diagram (dual grid) is then found according to the reciprocal relationship with the form diagram. Corresponding branches are parallel and branches which come together in a node in one of the networks form a closed polygon in the other and vice versa [9] (fig. 8). The lengths of the branches of the force diagram multiplied by the scale factor represent the magnitude of the horizontal components of the forces in corresponding branches in the thrust network. Corresponding to one form diagram, there may be infinite possible force diagrams. The indeterminacy of the force diagram will be discussed more fully later in 2.6.3.

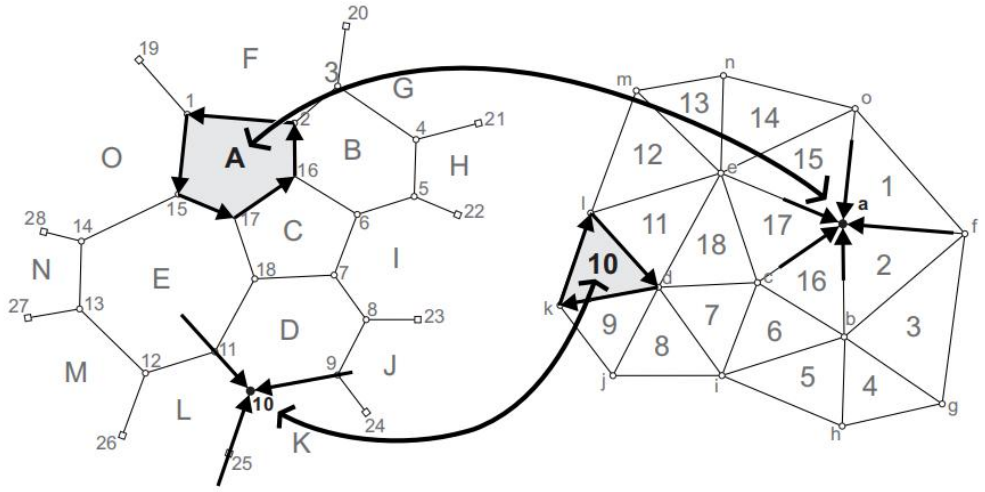

Fig. 8. The form diagram and the force diagram are related by a reciprocal relationship [13], and the notations here are adapted from Bow's rules [11].

3. With a form diagram and its corresponding force diagram obtained, the remaining unknowns are the heights of nodes and the scale factor of the force diagram. The constraints are the equilibrium equations at all nodes since all branches coming together per node need to be in equilibrium with the applied external loads. In the case of designing a new vault, the scale factor can be defined freely by the user, and then all the nodal heights can be calculated directly through solving the equilibrium equations. In the case of analyzing a historical vault, the scale factor, as well as the nodal heights, can be solved simultaneously by means of optimization methods to constrain all the nodes of the thrust network within the structure.

This method was proposed by Block [3, 20] and has been developed by the Block Research Group, Swiss Federal Institute of Technology in Zurich (ETH Zurich) [21]. It is a powerful method that can be used to not only design new free-form funicular vaults [22-24] but also analyze historical structures. However, in the case of analyzing historical structures, the given form diagram may not be feasible, rendering that no solution can be found through the optimization approach. That is to say, the results of this method largely rely on the experience and intuition of the analyst, who has to feed TNA an appropriate form diagram in the beginning. Unfortunately, this task can be very hard sometimes, for example, when encountering a structure of a complex shape.

2.6.2. Previous studies on defining the form diagram

As mentioned in section 2.6.1, using an appropriate form diagram is very important since the equilibrium solution and the force distribution are highly dependent on it [3]. Thus, in this section, several rules according to previous studies are introduced to advise how to construct a reasonable form diagram.

Many scholars have assumed that forces flow to the supports in the same manner as water would

drain off the vault's upper surface or as a cannonball would roll off the extrados of a vault (Fig. 4, left) [14]. However, this kind of pattern may not be reasonable for some vaults with open edges as the forces would directly hit on the open edges rather than flow to the supports.

Panozzo et al [25] proposed several heuristics to create form diagrams for vaults with open edges or creases. An example of a surface with an open edge and creases is shown in Fig. 9 where the blue line represents the open edge and red lines represent creases. He stated that forces should flow along the open edges and force lines are needed where creases occur in the geometry. For vaults with open edges, Block and Lachauer [26] also stated that the arch pattern may be an important feature of the form diagram to collect forces to the support. As shown in Fig. 10, for the example of a groin vault, the form diagram is generated through combining a regular quadrilateral grid and the arch pattern.

Fig. 9. The positions of the open edge (blue line) and the creases (red line) in the target surface [25]

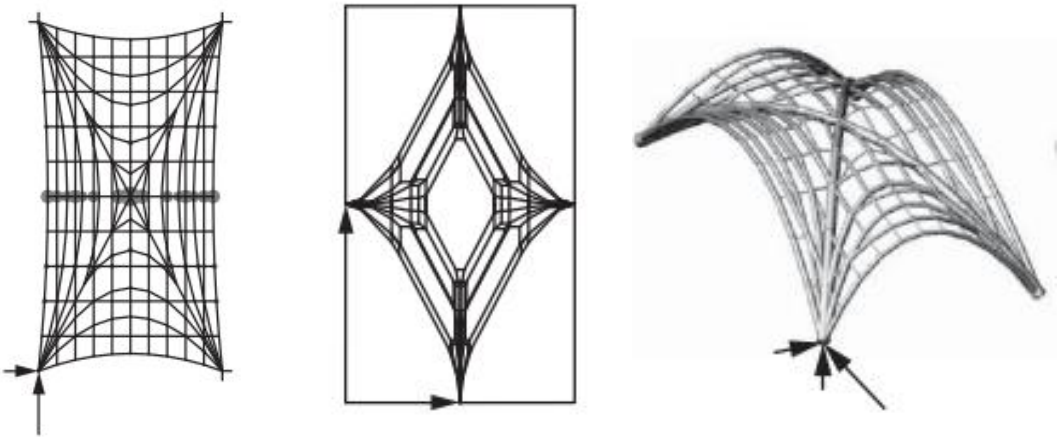

Fig. 10. The form diagram combining a regular quadrilateral grid and the arch pattern, its corresponding force diagram, and the thrust network [26]

O'Dwyer stated that the external forces can have an influence on the pattern of the form diagram. For example, for a barrel vault, the most basic way to conduct the analysis is to assume that the imposed loads are carried by independents arches (Fig. 11, left) [19]. Such an assumption is good enough when the vault is under self-weight only. However, when there is an additional point load, this assumption of force flow could be conservative because the point load is all carried by one single arch (Fig. 11, left). In contrast, a more appropriate pattern, which is shown in Fig. 11 right, allows utilizing more material to resist the external load. Apart from the influence of the external

forces, regarding the mesh density of the form diagram, O'Dwyer stated that using a denser mesh would result in more accurate results but more computational cost [19].

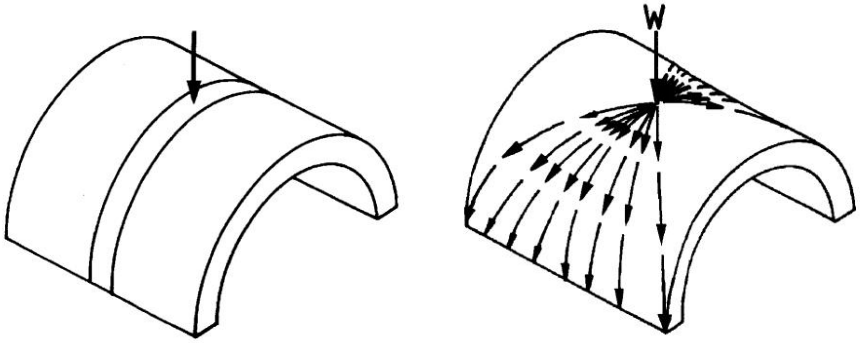

Fig. 11. Two different assumptions of load path for a barrel vault applied with a point load [19]

To deal with the point load, Block and Lachauer [27] proposed a method which is to combine the initial pattern, which was generated considering the self-weight only, with a radial pattern. The radial pattern, which radiates from the application location of the point load to the supports, provides appropriate force paths for the point load. Fig. 12 shows an example of a form diagram as well as its force diagram and thrust network, before and after adding the radial pattern at the application point of a load point. This method is also mentioned in [28].

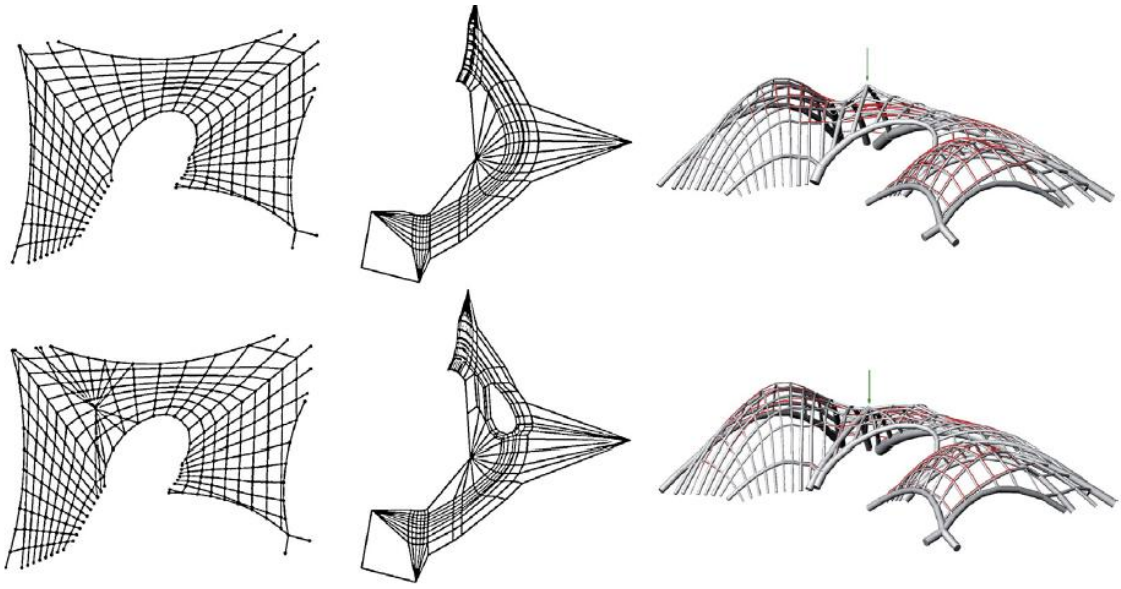

Fig. 12. Top, the initial form diagram, its corresponding force diagram, and the thrust network [27];
Bottom, the new form diagram with a radial pattern, its corresponding force diagram, and the thrust network [27].

Several rules regarding the form diagram are listed above and they are based on a large experience and deep insight of the authors. However, most of them have not been strictly and systematically verified and therefore, may only be appropriate for vaults of certain shapes. In addition, these rules all aim at masonry vaults, but the main research objects of this dissertation are composite vaults of

different shapes with additional reinforcements. Besides, the analysis methods are also different, and they may have different definitions of “a proper form diagram”. In this case, whether these rules can be well applied in this dissertation remains to be verified.

2.6.3. Indeterminacy of the force diagram

In this section, the indeterminacy of the form diagram is put aside to focus on the force diagram. A fixed form diagram is provided for the following discussions. Based on the fixed form diagram, the force diagram can be generated according to the reciprocal relationship (mentioned in section 2.6.1). If somehow, a force diagram can be transformed without violating the reciprocal relationship into a new one, that is to say, all branches are still in the same directions, then the new force diagram will be reasonable as well. Such transformations result in the indeterminacy of the force diagram.

First of all, any force diagram can be scaled (all branches expand or shrink by the same proportion) to create a new reasonable one, because such transformations will not change the directions of the branches. In Fig. 13, an example of scaling a random quadrilateral is provided. This one degree of freedom is represented by a parameter called “scale factor”.

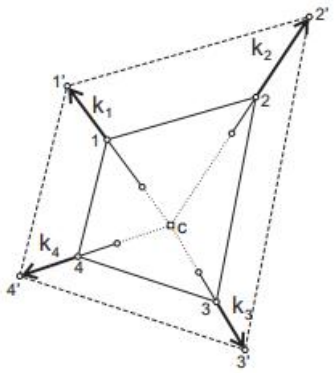

Fig. 13. Globally scaling the force diagram keeps all the branches in the same directions [3]

Then, with a fixed scale factor, depending on the pattern of the fixed form diagram, it can be divided into two situations. On the one hand, if all nodes in the form diagram are three-valent, which means that three branches come together at each point (as shown in Fig. 8, left), the force diagram will be uniquely defined. This can be understood through the shape of the force diagram (Fig. 8, right). The force diagram is triangulated, thus all the nodes are locked and only one shape exists except for the scale factor. On the other hand, if it is not the case above, there will be infinite possible force diagrams corresponding to the form diagram [3]. One simple example is listed below.

As shown in Fig. 14, for the same form diagram (on the left), some branches of the original force diagram (on the middle) are stretched forming the new force diagram (on the right). The lengths of these branches are different but the directions of which are of the same. This kind of

transformation does not violate the reciprocal relationship, thus the new force diagram is reasonable as well. In addition, in the same way but changing the magnitude of elongation, infinite new force diagrams can be generated.

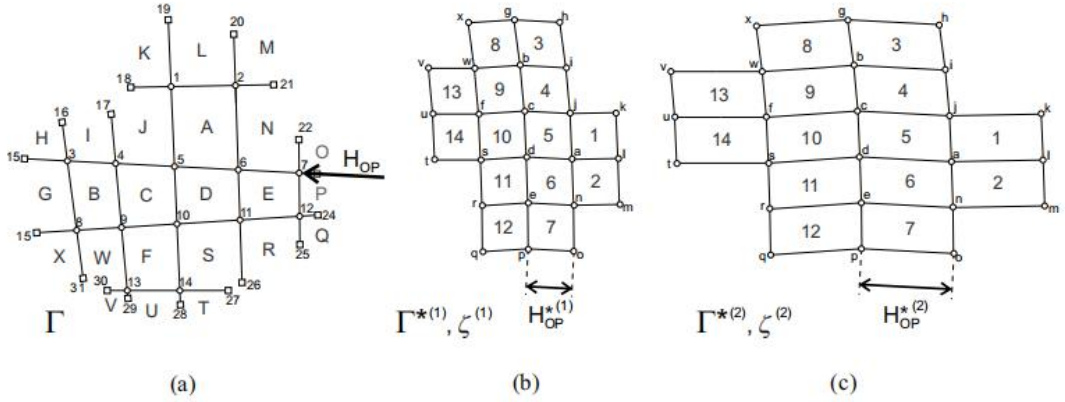

Fig. 14. Left, the original force diagram;
Right, a new force diagram with some branches stretched in the original direction [3].

In RhinoVault, which is a plug-in of Rhino based on the thrust network analysis developed by Rippmann et al. [21], users are able to manipulate the force diagrams by dragging points or stretching branches as desired. The program will automatically find the new force diagram, which is as parallel as possible to the one that the user wants, according to the reciprocal relationship. One example is shown in Fig. 15. The form diagram is fixed. Some branches of the original force diagram (on the top) are stretched to attract more forces forming a new one (on the bottom). Correspondingly, a crease is generated in the new thrust network.

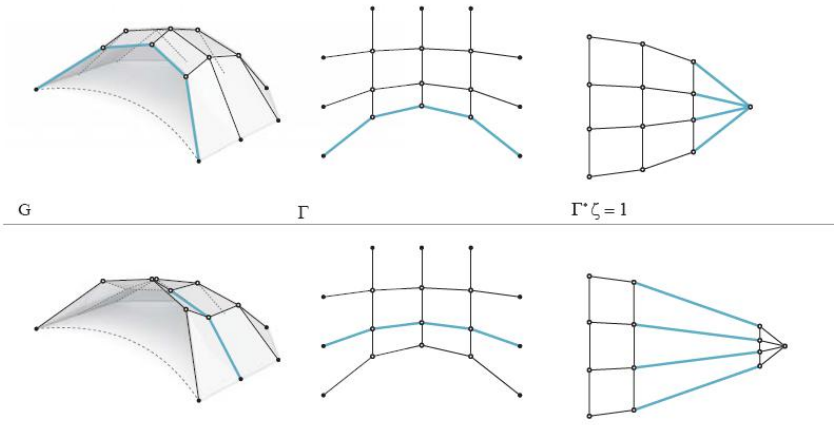

Fig. 15. Top, original form diagram, force diagram, and thrust network [21];
Bottom, the form diagram is the same, and some branches are stretched in the force diagram to attract more force, as a result, generating a crease in the thrust network [21].

2.6.4. The best-fit method

With a fixed form diagram, RhinoVault permits users to manipulate the nodes and branches of the

force diagram to explore different shapes of funicular shell structures. However, in the case of analyzing historical vaults, of which the objective is to find a thrust network that fits inside or as close as possible to the historical structure, manually dragging points or stretching branches to adjust the shape of the thrust network to fulfill the request could be very hard or even impossible. Therefore, a more sophisticated solution is needed.

With a fixed form diagram, the force diagram can be represented by force densities [29]. The force density is equal to the length of the branch of the force diagram divided by the length of the corresponding branch of the form diagram. Utilizing the force densities, the Block Research Group created the best-fit method [25-28] to find the closest thrust network to the mid surface of a target vault. With a given target surface, the solving procedures of this method are listed as follows:

1. Generate a starting point:

a. choose a form diagram;

b. generate an initial force diagram;

c. optimize the scale factor of the initial force diagram.

2. Find a best-fit solution by repeating the following two-step procedure until convergence:

a. find the force densities that minimize the distance between the target surface and the thrust network, ignoring the geometry constraints between the form and force diagrams;

b. for the current densities, find the force diagram that is as parallel as possible to the form diagram.

For detailed discussions of each step and its substeps, the author refers to reference [28].

One example of applying this method to obtain a best-fit thrust network is shown in Fig. 16. The closest thrust network (on the left) is generated based on the given form diagram (on the right). The radius of the blue circle at each node represents the remaining distance between the thrust network and the target surface (on the left, in grey). For detailed discussions and calculations, the author refers to the provided references.

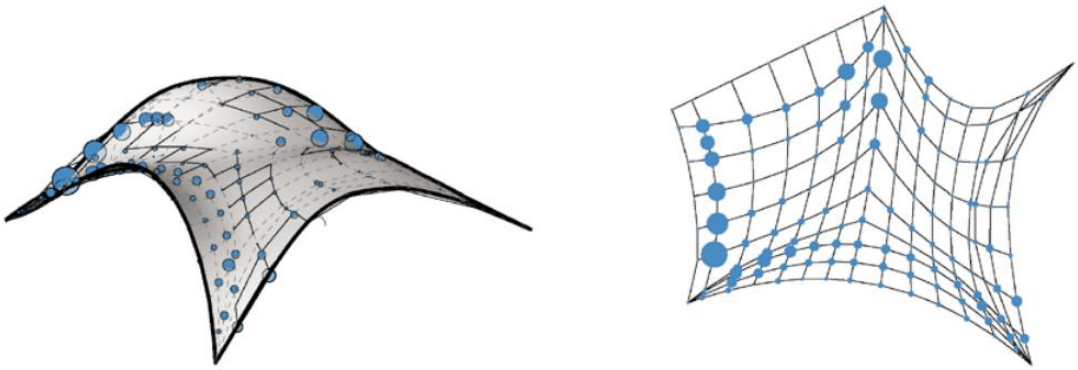

Fig. 16. Left, the best-fit thrust network and the mid surface of the target vault [28];
Right, the form diagram of the best-fit thrust network, where the radiuses of the blue circles represent the distances between the thrust network and the mid surface [28].

2.7. Extended limit analysis for reinforced masonry

Thrust network analysis (TNA) has an outstanding performance for designing new funicular vaults and analyzing historical structures. However, it can only be applied to pure compression vaults. For vaults with some regions in tension that can be resisted either by the tensile strength of the material or additional reinforcement, TNA cannot finish the analysis without complementary tools.

Roca et al. [30] proposed a method and a tool to analyze reinforced masonry or concrete arches. The method is based on limit analysis (mentioned in 2.3) and uses the safe and the uniqueness theorems, together with an optimization process, to determine the ultimate capacity of the structures. Instead of using the real boundary of the structures as the geometrical constraints, this tool uses the "strength boundary" which represents the maximum possible eccentricity of the resultant force in the cross-section. The position of the strength boundary depends on the amount of reinforcement and its position, the thickness of the cross-section, and the compressive strength of the material. With this information, a conventional cross-sectional analysis will allow us to obtain the position of the strength boundary. For detailed procedures, the author refers to the provided references.

However, this method can only be used for singly-curved vaults that can be simplified into a plane problem. For a vault whose three-dimensional behavior is difficult or impossible to be simplified, for example, a dome, a sail vault, or a bizarre free-form vault, this method cannot be well applied.

Based on Roca, López López conducted a more in-depth analysis and created the Extended Limit Analysis for Reinforced Masonry (ELARM) [1, 2]. ELARM allows to design and analyze two- or three-dimensional reinforced concrete, masonry, and composite shells of most shapes. ELARM3D [2], the three-dimensional version of ELARM, incorporates the method proposed by Roca et al. into the framework of thrust network analysis (TNA), enabling the design and analysis of partially tensioned shells. The main steps of ELARM3D are stated as follows.

First of all, the mesh of the mid surface of the target vault, as well as necessary material properties information, needs to be provided by the user. A form diagram is also needed, which is the same as for TNA. Then, a force diagram can be automatically generated based on the algorithms of TNA, and a thrust network can be constructed as well with these two planar diagrams.

Then, the form diagram is vertically projected into the mid surface of the target vault. In the cross-section at the midpoint of each branch in the mid surface, the virtual boundary (strength boundary) can be calculated through cross-sectional analysis with the resultant force obtained from the thrust network and the already given material properties.

For the cross-sectional analysis, the first step is to identify the strain domain. Four different strain domains are defined in ELARM3D. Each strain domain indicates a different stress-strain state of the materials and corresponds to a different system of equations to solve the cross-section equilibrium. The borders of these domains are determined according to the deformation compatibility equations. The strain domain can be identified according to the neutral axis position, which can be obtained by solving the force equilibrium of the axial force, the compression by concrete, and the tension by reinforcement. Before that, the assigned width and allocated steel amount for the cross-section need to be calculated according to the form diagram, the vault’ s geometry, and the arrangement of steel bars. The axial force is also required from the thrust network. After the computation for each strain domain, four results are obtained. However, some of them may not lie inside the corresponding domain’s borders. Thus, those unmatched results are neglected, and only one unique ultimate strain-stress state will be determined. For the last step, knowing the strain domain, based on the moment equilibrium, the axial force’s eccentricities, both for the positive and negative moment, can be calculated. Thus, the virtual boundaries are found out. For the detailed equations and calculation process, the author refers to reference [1, 2].

In the end, ELARM3D checks if the thrust network fits inside the virtual boundary. Being so means the structure is safe, otherwise, no one can say anything about the safety of the vault, unless all the possibilities of the form diagram and the force diagram have been systematically tested. Finding any thrust network in equilibrium with the external loads and lying within the virtual boundary is sufficient to ensure stability.

Beyond pure compression vaults, ELARM can be used for the analysis and the design of two- or three-dimensional reinforced concrete, masonry, and composite shells of most shapes. The form diagram in ELARM (based on TNA) should be provided by the user. As mentioned above, choosing an appropriate form diagram may not be straightforward and the quality of the form diagram can have an enormous influence on the results obtained through ELARM.

3. METHODOLOGY

3.1. Introduction

As mentioned in section 2.7, ELARM3D allows the design and analysis of a reinforced vault. However, it cannot directly determine the least amount of reinforcement for a given form diagram, as many parameters influence the amount of reinforcement simultaneously.

For ELARM3D, the required inputs are listed as follows. The form diagram, the thickness of the concrete layer *hc*, the direction of the steel bars θ, the separations between the steel bras in both directions *sep1* and *sep2*, the reinforcement position *t*, the steel bar areas in both directions *As1* and *As2*, the young's modulus of concrete *Ec*, the compressive strength of concrete *fc*, the young's modulus of steel *Es*, the tensile strength of steel *fs*, the maximum compressive strain of concrete *ecmax*, the maximum tensile strain of steel *esmax*, the height of the thrust network *h*, the application point of the external loads, the magnitude of the external loads, the density of concrete *dc*, and other parameters that are not in the scope of this research, thus, are neglected here.

Among these parameters, the form diagram is considered to be fixed in this chapter; *hc* is always restricted by other factors, for example, aesthetic, thus considered to be fixed; *sep1* and *sep2* are assumed to be fixed and of the same value in this research; *As1* and *As2* are assumed to be the same, and for the following discussion, *A* is used to represent the steel bar area; *Ec*, *fc*, *Es*, *fs*, *ecmax*, *esmax*, and *dc* are material properties, and are considered to be fixed in this research; the application points and magnitudes of external loads correspond to the load case, which is already given for the design. In summary, the remaining variables for the vault's design are θ, *t*, *h*, and *A*.

In this research, *A* is used to represent the total steel amount because *sep1* and *sep2* are fixed, and the total steel amount is only influenced by *A* for a vault of a given geometry.

To reduce the reinforcement usage, a method is needed to find the best set of θ, *t*, and *h*, such that *A* reaches the minimum for a given form diagram. These three key parameters θ, *t*, and *h* are focused on and discussed in the following sections. How each key parameter functions in the calculation process is introduced in section 3.2. An algorithm to optimize these three key parameters to determine the least amount of reinforcement for a fixed form diagram is presented in section 3.3, together with an application example of this method and its pros and cons.

3.2. The influence of each key parameter

3.2.1. The height of the thrust network, *h*

As mentioned in section 2.6.3, the force diagram can be scaled, and this one degree of freedom is represented by the scale factor. Increasing the scale factor means scaling up the magnitude of all horizontal forces in the system, leading to a lower height of the thrust network. On the contrary,

decreasing the scale factor will function the other way around. In ELARM3D, the height of the thrust network, h, which is equivalent to the scale factor, is used to control the scale of the force diagram.

As mentioned in section 2.7, the virtual boundary represents the axial force's maximum possible eccentricity in the cross-section. For the ultimate equilibrium state, the bending moment caused by the eccentricity of the axial force is resisted by the concrete and the reinforcement. A smaller axial force is allowed for a larger force arm, i.e., eccentricity, which is also the virtual boundary, and vice versa.

As a summary of the above discussions, increasing h raises the thrust network and deceases the thrust network branches' forces, rendering the range of virtual boundary broader, and decreasing h does inversely.

An appropriate value of h is necessary. If it is too large, though the branches' forces are small and the range of the virtual boundary is broad, some branches may still cross the upper virtual boundary, thus violating the safety theorem. On the other hand, h should not be too small as well. In that case, the forces are extensive in the thrust network, causing the virtual boundary range to be so narrow that some branches below the mid surface cannot reach the lower virtual boundary.

3.2.2. The position of the reinforcement, t

The position of the reinforcement, t, is defined by the distance between the steel bar and the upper surface of the structure in the cross-section. Increasing t means placing the reinforcement at a lower position, thus allows a larger maximum eccentricity of the axial forces above the steel bar (the upper virtual boundary) but a smaller maximum eccentricity below it (the lower virtual boundary). On the contrary, decreasing t represents placing the steel bar closer to the upper surface, thus provides a narrower upper virtual boundary and a wider lower virtual boundary.

In practice, if ELARM3D shows an error that several branches go beyond the virtual boundary from one side, either the upper one or the lower one, adjusting t can be a possible method to solve the problem. However, if both the upper and lower virtual boundaries are crossed, merely changing t cannot help. Other parameters should be adjusted as well.

3.2.3. The direction of the reinforcement, θ

In this dissertation, the reinforcement is considered to be in the form of steel mesh. The projection of the mesh in the horizontal plane is square grids. Steel bars are placed in two perpendicular directions, and the spaces between steel bars of both directions are the same. The direction of the reinforcement, θ, is defined as the smaller angle between the y axis and the steel bar of one direction in the horizontal plane. Due to the rotational symmetry of square grids (they look the

same after rotating 90°*n, where n can be any positive integer) , the range of θ is [-45°, 45°].

ELARM3D contains the algorithm to calculate the allocated steel amount for each branch in the vault's mid surface. One crucial part of this algorithm is to find the new angle between the projected steel bars and the new angles between the cast steel bars and the branches. The variation of angles is due to the vertical projection of the square grids from the horizontal plane to the vault's mid surface. Based on θ and the vault's geometry, one can calculate these new angles by applying mathematical knowledge of spatial geometry. Together with these new angles, the algorithm takes into account the assigned width for the branch's cross-section and the steel bar area to compute the final result.

As can be known from the above introduction, θ plays a critical role in calculating the allocated steel amount for each branch in the mid surface, thus directly influences the required amount of reinforcement.

To find the best value for θ such that the required reinforcement amount can reach the minimum, there are two approaches:

The first one is to check the statuses of all the branches in the mid surface, including their axial forces and the positions of their corresponding branches in the thrust network. Then, based on these information, one can calculate the allowable range of θ that renders for the part of this branch, the thrust network fit inside the virtual boundaries. Afterward, the intersection of all allowable ranges is determined as the feasible range of θ. In this range, any value of θ would ensure all the branches to be in a safe state. To find the best value for θ, the reinforcement amount needs to be decreased, and the feasible range should be recalculated until it contracts into a point. By then, the best value for θ is found to be that point. However, this method involves a large amount of calculation, being unwieldy and tedious.

The second method is a numerical one. Thanks to the square girds' rotational symmetry, the range of θ is limited to [-45°, 45°]. One can go through all the points after discretizing this range by a proper space. Then, for each point, the required reinforcement amount can be obtained. The one corresponding to the least amount of reinforcement will be the best value for θ.

3.3. A method to determine the least amount of reinforcement

3.3.1 Main steps

In practice, these three key parameters work together. To find the best combination of h, t, and θ such that the required reinforcement amount can reach the minimum, an iterative search method is proposed in this section. The flowchart of this method is shown in fig. 17. Generally speaking, several rounds of the iteration are needed to reach convergence. For each step of the

iteration, the feasible range, in which any point of the corresponding parameter would ensure the thrust network to lie inside the virtual boundaries, is found first. Then the midpoint of the feasible range is adopted to update this parameter. Here, the midpoint rather than the optimal point is chosen. This is to increase the calculation efficiency, as searching for the optimal point requires testing all the points, increasing much computation cost. However, when the iteration process converges, the reinforcement amount may not reach the minimum as it corresponds to midpoints, which may not be the optimal ones. Therefore, a fine-tuning step is needed after the iteration process to find the optimal parameters as well as the least amount of reinforcement.

In this dissertation, the reinforcement amount is represented by the cross-sectional area of steel bars, A. Since the spaces between steel bars are fixed, for a vault of given geometry, the total amount of steel is only influenced by A.

The detailed introduction of each step of this method is listed as follows.

First of all, a form diagram should be provided by the user. Initial values of these three key parameters $h(0)$, $\theta(0)$, and $t(0)$ are also needed to start the iteration. For θ and t, the midpoints of their ranges can be good choices for the initial values. For h, according to own experiences, it is recommended to assign h as around two times of the real vault height. With the above information, one can obtain the initial $A(0)$, which is the minimum value at this moment that renders the thrust network to lie inside the virtual boundaries.

For the first step of the iteration, with $\theta(\mathrm{i})$, $t(\mathrm{i})$, and $A(\mathrm{i})$ (i+1 represents the order of the current iteration round, for example, for the first round of iteration, i equals 0), the maximum value and the minimum value of h that keep the structure in the safe state can be obtained. Adopting any value inside the range $[h_{\min}, h_{\max}]$ would satisfy the safety theorem. This range is called the *feasible range*. To continue the iteration, the midpoint of this range is assigned to $h(\mathrm{i+1})$, so that $h(\mathrm{i+1})$ equals $(h_{\min}+h_{\max})/2$.

The second step is to update θ with $h(\mathrm{i+1})$, $t(\mathrm{i})$ and $A(\mathrm{i})$. As mentioned above, a numerical method to test all the possible values of θ can be effective. Thanks to the square grids' rotational symmetry, the range of θ is limited to [-45°, 45°]. An appropriate space can be defined to discretize this range into multiple points, and then all points should be tested. Feasible points, which enable the thrust network to lie inside the virtual boundaries for the current reinforcement amount, are picked out according to the results. Then, the point of the median number is assigned to $\theta(\mathrm{i+1})$. If the number of feasible points is even, either of those two points near the median number can be assigned to $\theta(\mathrm{i+1})$.

The third step is to deal with t. With $h(\mathrm{i+1})$, $\theta(\mathrm{i+1})$, and $A(\mathrm{i})$, the feasible range of t can be found. $t(\mathrm{i+1})$, then, is determined as the midpoint of this range.

For the fourth step, A(i+1) can be found. It is the latest minimum reinforcement amount based on the updated values of h(i+1), θ(i+1), and t(i+1).

In the end, the algorithm compares A(i) with A(i+1). If A(i+1) is smaller than A(i), the algorithm will go back to the first step and conduct the iteration again to reach a lower value of A. If A(i+1) is equal to A(i), this indicates the iteration's convergence. A(i+1) cannot be larger than A(i), because if so, the combination of h(i+1), θ(i+1), t(i+1), and A(i) will violate the safe theorem, as A(i+1) is the minimum value for the cross-sectional area at the current moment. However, this conflicts with the fact that at the end of the third step, the combination of h(i+1), θ(i+1), t(i+1), and A(i) satisfies the safe theorem.

In this way, each step of the iteration drives A to be smaller or unchanged, and a lower value of A also narrows the feasible range of these three parameters. In the end, after several rounds of iteration, A reaches convergence, and the feasible ranges of the key parameters also contracts significantly.

However, for now, it is unsure whether A reaches the lowest value because the midpoints of the feasible ranges assigned to update h, θ, and t may not be optimal. Thus, a final fine-tuning step is needed to test all possible points to find the optimal ones. It is also an iteration process. Firstly, one can fix h and θ to find the feasible range of t, and then test all the points of t in this range to find the optimal one, and update t with this optimal value. Afterward, conduct the same process for h and θ to find the optimal values of their own. In this way, all the optimal parameters can be found as well as the least amount of reinforcement. Besides, for this step, the feasible ranges are narrow due to the low value of A, so the computation cost of testing all the possible points is acceptable.

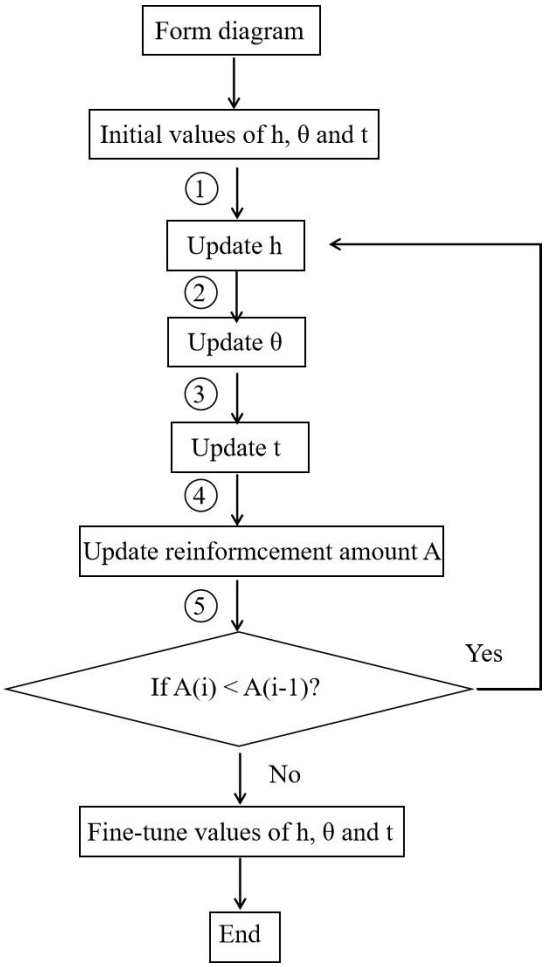

Fig. 17. The flow chart of the iterative search method

3.3.2 An example of application of the method

This section provides an example to illustrate how to use this method to find the least reinforcement amount for a given form diagram.

The vault to be analyzed is a reinforced concrete sail dome whose mid surface is provided in fig. 18. The span of the vault is 1.76m, and its height is 0.4m. The load case is self-weight only.

Values of related parameters are shown in table 1:

The thickness of the concrete vault	0.090m
Distances between steel bars in both direction	0.08m
Young's modulus of concrete	35000MPa
Compressive strength of concrete	25MPa
Young's modulus of steel bars	210000MPa
Yield strength of steel bars	500MPa

The maximum compressive strain of concrete	0.0035
The maximum tensile strain of steel bars	0.01
The density of the concrete	2460kg/m^3

Table 1. Values for related parameters

The form diagram is provided, as shown in fig. 19 left. It contains a simple rectangular grid pattern. The force diagram is generated automatically by the embedded algorithm, as shown in fig. 19, right.

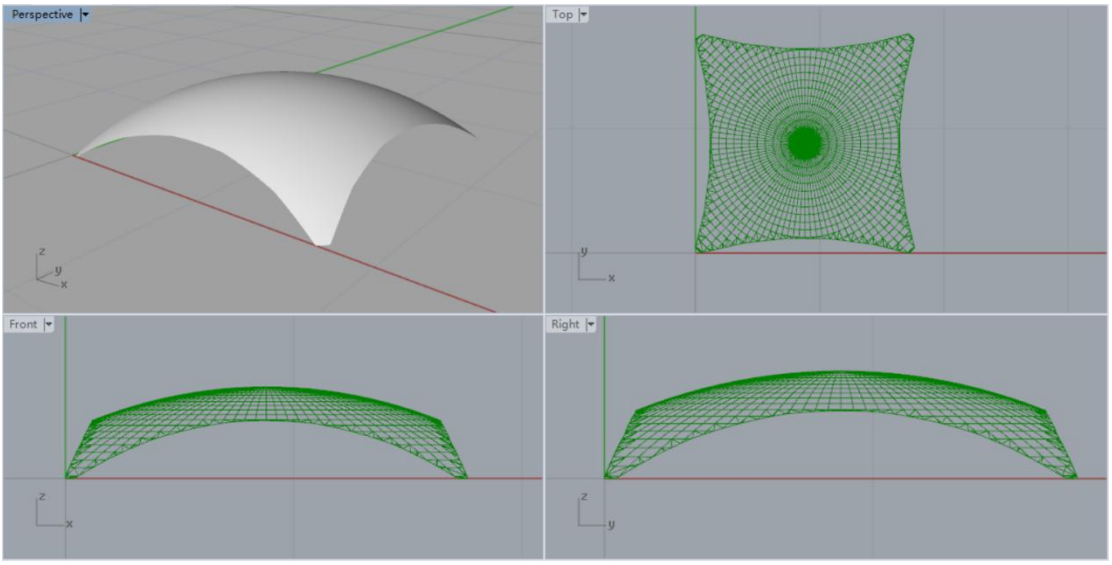

Fig. 18. Perspective view (left top), top view (top right), front view (bottom left) and right view (bottom right) of the mid surface of the sail dome

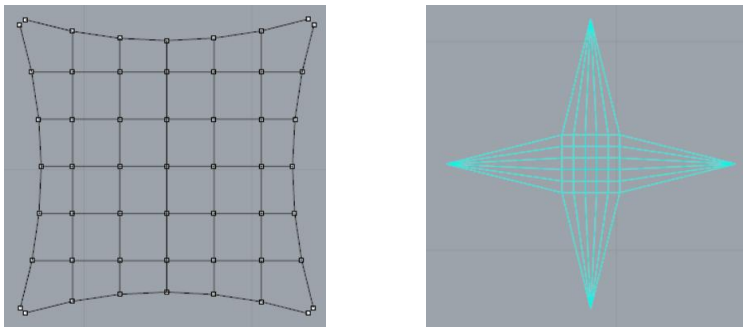

Fig. 19. The user-given form diagram (left) and the program-generated force diagram (right)

The processes and data are shown in table 2. First of all, random initial values are assigned to three key parameters. In this example, $h(0)$ is equal to 1m, $\theta(0)$ is equal to 0° and $t(0)$ is equal to 0.045m. Based on these three parameters, $A(0)$ is found to be 0.00100 cm^2.

Then, the algorithm conducts the first round of iteration. For the first step, with $\theta(0)$ equal to 0°, $t(0)$ equal to 0.045m and $A(0)$ equal to 0.00100cm^2, the feasible range of h is obtained to be [0.73, 1.00]. The midpoint of this range, 0.87, is then assigned to $h(1)$.

The second step is to find feasible points of θ. It turns out to be that all points ({-45°, -40°, -35° ... 40°, 45°} with 5° adopted as the space in this example) are proper, thus the midpoint, 0°, is assigned to $\theta(1)$.

For the third step, the feasible range of t is obtained to be [0.037, 0.89] so that $t(1)$ equals 0.063.

The final step of the first round of iteration is to find the current minimum A that satisfies the safety theorem. The result of $A(1)$ is 0.0059. At the end of the first round of iteration, comparing $A(1)$ to $A(0)$, a significant reduction is observed, thus the algorithm jumps into the second round to seek for a further possible reduction in A.

In this example, six rounds of iteration in total are conducted. The procedures in each round are similar to those in the first round. In the sixth round, $A(6)$ is 0.00038, which is the same as $A(5)$, indicating the iteration process's convergence. However, $A(6)$ may not be the best value for A, as only midpoints are used to update h, θ, and t, while they are possibly not the best ones in the feasible ranges. Therefore, all the values in the final feasible ranges need to be tested to find the optimal ones. This step is the so-called fine-tuning step. Eventually, the best results are found. h is equal to 0.78 m, θ is equal to 0° (actually, any value of θ is fine, which may due to that the influence of θ on the results is slight for this example), t is equal to 0.089 m, and A is equal to 0.00035 cm^2.

	h/m		θ/°	t/m		A/cm²
Initial value	1.00		0	0.045		0.00100
1	0.73	1.00				
	0.87		all			
			0	0.037	0.089	
				0.063		0.00059
2	0.77	0.87				
	0.82		all			
			0	0.058	0.089	
				0.074		0.00046
3	0.77	0.82				
	0.80		all			
			0	0.071	0.089	
				0.080		0.00041
4	0.78	0.80				
	0.79		all			
			0	0.077	0.089	
				0.083		0.00039
5	0.78	0.80				
	0.79		all			
			0	0.081	0.089	
				0.085		0.00038
6	0.79	0.80				
	0.80		all			
			0	0.085	0.089	
				0.087		0.00038
Fine-tune	0.78		all	0.089		0.00035
End	0.78		0	0.089		0.00035

Table 2. The detailed process of applying the method to obtain the least amount of reinforcement

3.3.3 Pros and cons

Pros:

This method has a simple structure and is easy to operate. Thanks to the high calculation efficiency of ELARM3D, this method can be applied by hand, as it only takes seconds to obtain the results after changing the values of parameters. Besides, this algorithm can be coded to allow automatic calculation for the iteration process and the fine-tuning step, which can realize even higher calculation speed. This method is also robust as the iteration process will always converge because A(i+1) will never be larger than A(i), which is already proved in section 3.3.1.

Cons:

The results obtained are local optima, as it is related to the initial values of parameters. In practice, to obtain the global optima, it is advised to try with different sets of initial values, especially for h, and then compare the results. The minimal A obtained among them is considered as the global minimum.

4. THE INFLUENCE OF THE MODEL NETWORK ON THE REINFORCEMENT AMOUNT

In this chapter, different form diagrams (the horizontal projection of the thrust network, as mentioned in section 2.6.1) are explored for vaults of basic shapes under several different load cases.

For the vault shapes and the load cases, seven combinations are investigated in this research:

1. Mesh 1 + Load case 1
2. Mesh 1 + Load case 2
3. Mesh 1 + Load case 3
4. Mesh 2 + Load case 1
5. Mesh 2 + Load case 2
6. Mesh 3 + Load case 2
7. Mesh 4 + Load case 2

Where,

Mesh 1 (fig. 20): The mid surface of a reinforced concrete sail dome with a span of 1.76 m and a height of 0.40 m.

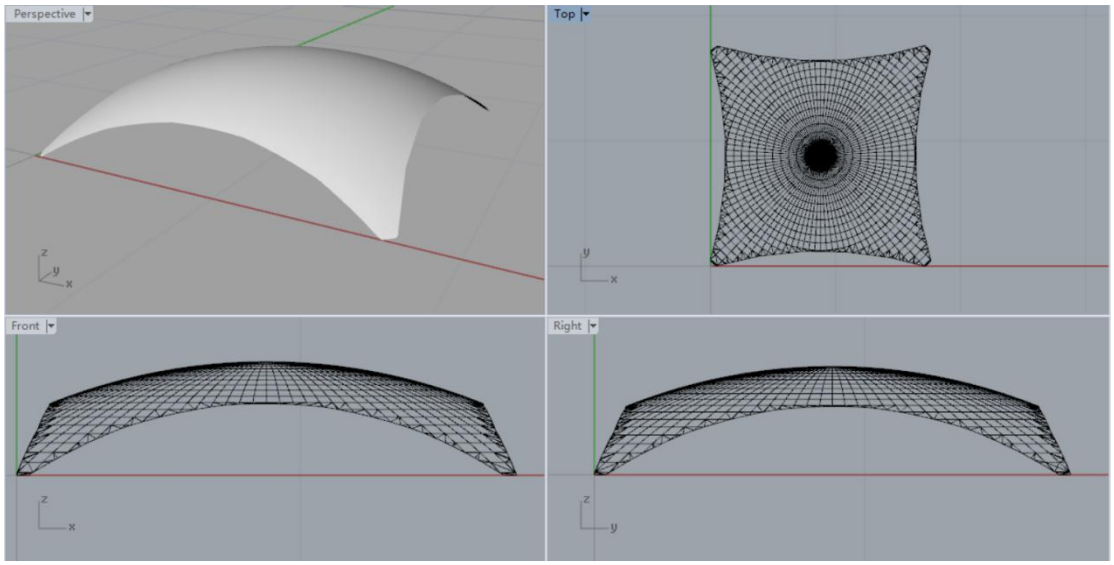

Fig. 20. The perspective view (left top), top view (top right), front view (left bottom), and right view (right bottom) of mesh 1

Mesh 2 (fig. 21): The mid surface of a reinforced concrete sail dome with a span of 1.76 m and a height of 1.05 m.

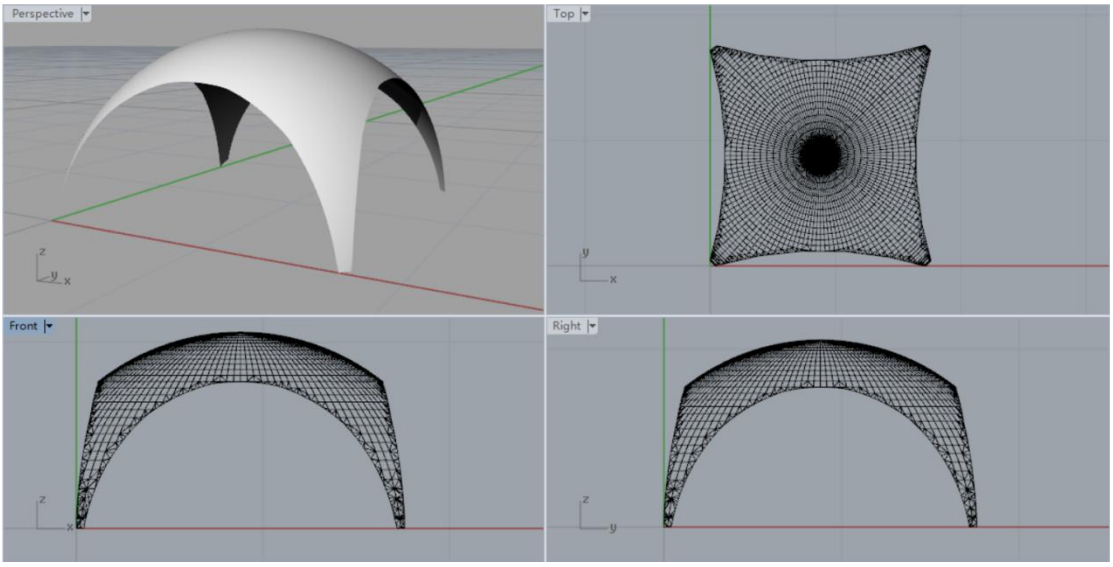

Fig. 21. The perspective view (left top), top view (top right), front view (left bottom), and right view (right bottom) of mesh 2

Mesh 3 (fig. 22): The mid surface of a reinforced concrete semi-spherical dome with a radius of 3 m.

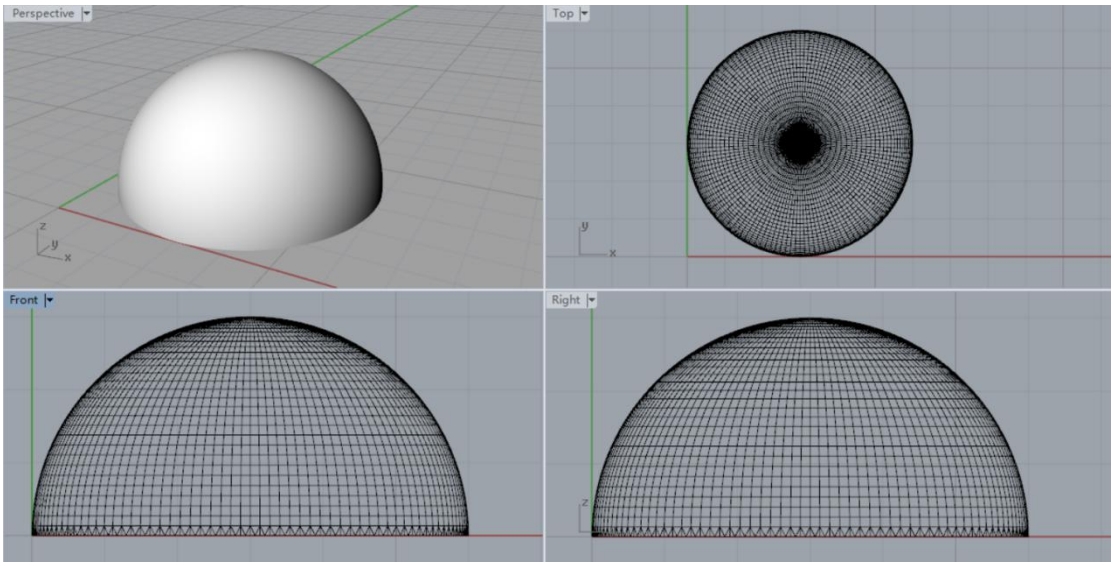

Fig. 22. The perspective view (left top), top view (top right), front view (left bottom), and right view (right bottom) of mesh 3

Mesh 4 (fig. 23): The mid surface of a reinforced concrete semi-spherical dome with a radius of 6 m.

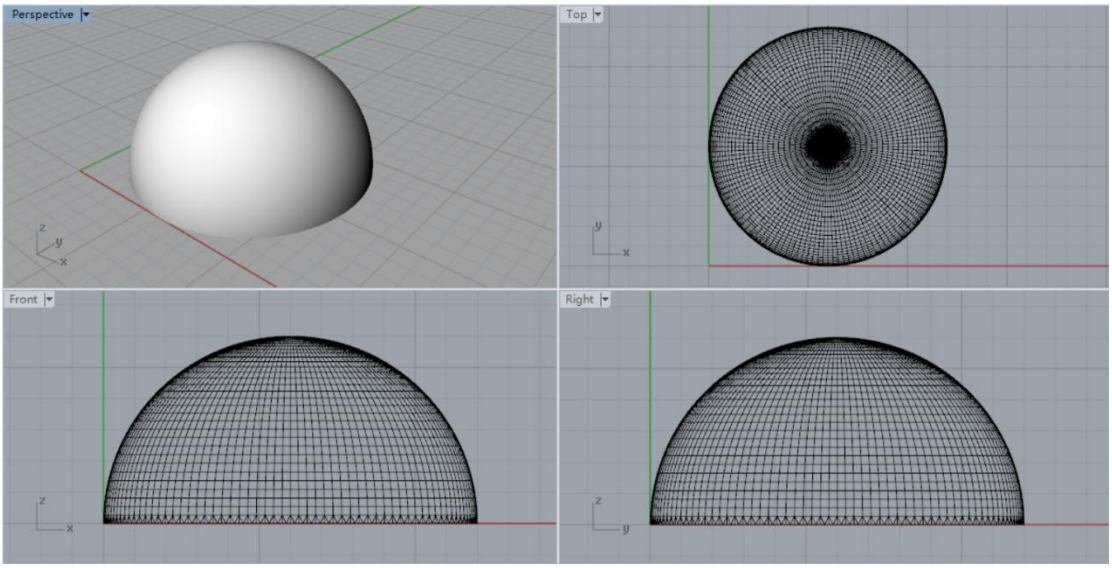

Fig. 23. The perspective view (left top), top view (top right), front view (left bottom), and right view (right bottom) of mesh 4

Load case 1 - self-weight only
Load case 2 - self-weight + one point load (2kN) at the midpoint of the vault
Load case 3 - self-weight + one point load (2kN) at a specific point on the vault

For each combination, multiple form diagrams are explored. Each individual study case consists of the geometry of the vault, the load case, the form diagram, the force diagram, the height of the thrust network h, the direction of the reinforcement θ, the position of the reinforcement t, and the necessary reinforcement amount A.

For each case,
the geometry of the vault and the load case are assigned by the author;
the form diagram is designed by the author;
the force diagram is generated automatically through the algorithm embedded in ELARM3D based on TNA;
the best set of h, θ, and t, as well as A, is obtained through the method presented in chapter 3.

The rest parameters are assigned with constant values listed in table 3 for all cases useless otherwise specified.

The thickness of the concrete vault	0.090m
Distances between steel bars in both direction	0.08m
Young's modulus of concrete	35000MPa
Compressive strength of concrete	25MPa
Young's modulus of steel bars	210000MPa

Yield strength of steel bars	500MPa
The maximum compressive strain of concrete	0.0035
The maximum tensile strain of steel bars	0.01
The density of the concrete	2460kg/m^3

Table 3. Values for related parameters

The form diagrams, force diagrams, and detailed results for all combinations are provided in the corresponding sections (table A-1 - A-14) in the Annex.

5. CONSIDERATION OF THE NUMERICAL RESULTS

To investigate the influence of the form diagram's pattern on the necessary reinforcement amount, the numerical results for the seven combinations of mesh types and load cases are discussed in detail. Based on the comparisons between the results of specific study cases, the comprehensive analysis is presented in corresponding sections in the Annex.

Based on the numerical results obtained by ELARM3D of the current version, some rules are discovered:

1. Generally, form diagrams generated by superimposing additional patterns with the basic grid pattern result in more reinforcement than the one with a grid pattern. Besides, from the force distributions' perspective, the added force paths usually take up little force. However, there are some exceptions. Several form diagrams with additional force paths result in less reinforcement, and in contrast, their force diagrams show that the added force paths do attract a certain amount of forces.
2. For the same pattern, the one with a higher density typically results in more reinforcement than the loose one.
3. The pattern adapted from the grid pattern by curving the straight lines inwards, for example, form diagram 2.11 and 6.9 in the Annex, normally present better results than the original grid pattern.

After deeper consideration of the numerical results, it is realized that the necessary reinforcement amount is affected by, apart from the parameters discussed in chapter 3, three factors:

1. The rationality of the force paths in the form diagram. This represents the quality of the form diagram and is characterized by the pattern, i.e., the geometry and topology of the form diagram.
2. The calculation process of ELARM3D. As introduced in section 7.1, a simple method is proposed to calculate each branch's assigned width to obtain the assigned reinforcement. However, to what extent this method can reflect the structure's real behavior and how it influences the necessary reinforcement amount, the problems remain to be solved.
3. The force distribution. As stated in section 2.6, infinite force diagrams correspond to one form diagram. The force diagrams in this dissertation are generated by the embedded algorithm in ELARM3D based on TNA. However, such an algorithm does not consider the reinforcement amount, thus generating a random force diagram. As a result, the force distribution may not be reasonable for the provided force paths and the external loads, rendering the results conservative.

The numerical results are affected by all these three factors, so it is hard to identify how the form diagram influences the results without excluding the other two factors.

6. CONCLUSIONS AND FUTURE WORK

6.1. Conclusions and recommendations

An algorithm based on ELARM3D is proposed in this dissertation to search for the optimal values of the steel bar direction, the reinforcement position, and the thrust network height to determine the least amount of reinforcement for a given form diagram. This algorithm is robust and is sure to converge to a solution.

A series of form diagrams are investigated for several vaults of various geometries under multiple load cases. The numerical results reveal that the necessary reinforcement amount is influenced not only by the pattern of the form diagram but also by the calculation process of ELARM3D and the force diagram, i.e., force distributions in the form diagram. These factors significantly increase the complexity of the problem and remain to be studied.

Nevertheless, based on the obtained results, some recommendations can be provided for the users of ELARM3D of the current version regarding how to build a proper form diagram to obtain a good result, i.e., relatively low necessary reinforcement amount:

1. A grid pattern, for example, form diagram 1.1 and 6.1 (in the Annex), is easy to generate and can be widely applied to the vaults of different geometries under different load conditions. Forces are assumed to flow to the supports in two perpendicular directions (except for the forces along the edge arches) in the structure. Generally, the required reinforcement amount for a grid pattern stays relatively low, according to the numerical results. Therefore, this pattern can be a proper choice for most cases. Besides, it can also work as an excellent starting point to be adapted into more sophisticated patterns.
2. For the same pattern, higher density typically results in more reinforcement, according to the numerical results. However, a sparse mesh may fail to fully capture the structure's behavior, leading to a deceptive result. When determining the density of a pattern, one needs to counterbalance the rationality of the pattern and the reinforcement amount.
3. Straight lines in the grid pattern can be modified to be curved inwards, rendering the areas of quadrilaterals more uniform and forming a series of arches to collect forces. Such patterns, for example, form diagram 2.11 and 6.9 in the Annex, generally present better results than standard grid patterns.
4. For the load case of a point load, based on a grid pattern, one can add additional force paths from the position where the point load is applied to the supports. However, for these additional force paths, one must check the force diagram, as it may be unreasonable. For example, the additional branches added to attract forces may be allocated with little force, as observed in case 2.9, 2.14, 2.18, etc. in the Annex. Unreasonable force distributions may lead to more conservative results. In that case, it is better to omit these additional patterns.

6.2. Future work

To improve the algorithm and exclude the external factors influencing the reinforcement amount, some possible future works are proposed as follows.

1. The algorithm proposed in chapter 3 can be coded and integrated into ELARM3D so that higher computational efficiency can be achieved. Besides, the algorithm should be improved to obtain the global optimum, as for now, the solution is affected by the initial values.
2. To avoid the force distribution's influence on the reinforcement amount, the most suitable force distribution needs to be determined. The best-fit method (in section 2.6.4) proposed by the Block Research Group provides a basic framework to solve this problem. In the method, the force densities are utilized to represent the force distribution, and are optimized to minimize the distance between the target surface and the thrust network. Inspired by this idea, one can manipulate the force densities to minimize the reinforcement amount by integrating the best-fit method with ELARM3D.
3. The influence of the calculation process of the assigned width on the reinforcement amount is unknown. More research is needed to verify this process or find a better solution.

REFERENCES

[1] López López D., Roca, P., Liew, A., Van Mele, T. and Block, P., 2019. Tile vaults as integrated formwork for reinforced concrete: Construction, experimental testing and a method for the design and analysis of two-dimensional structures. *Engineering Structures*, *188*, pp.233-248.

[2] López López D., 2019. *Tile vaults as integrated formwork for concrete shells: Construction, experimental testing, structural analysis and design* (Doctoral dissertation, ETH Zurich).

[3] Block, P.P.C.V., 2009. *Thrust network analysis: exploring three-dimensional equilibrium* (Doctoral dissertation, Massachusetts Institute of Technology).

[4] Heyman, J., 1966. The stone skeleton. *International Journal of solids and structures*, *2*(2), pp.249-279.

[5] Stevin, S. and Crone, E., 1955. *Principal works* (Vol. 2). CV Swets & Zeitlinger.

[6] Block, P., DeJong, M. and Ochsendorf, J., 2006. As hangs the flexible line: Equilibrium of masonry arches. *Nexus Network Journal*, *8*(2), pp.13-24.

[7] Culmann, K., 1875. *Die graphische Statik* (Vol. 1). Meyer & Zeller (A. Reimann).

[8] Beghini, L.L., Carrion, J., Beghini, A., Mazurek, A. and Baker, W.F., 2014. Structural optimization using graphic statics. *Structural and Multidisciplinary optimization*, *49*(3), pp.351-366.

[9] Maxwell, J.C., 1864. XLV. On reciprocal figures and diagrams of forces. *The London, Edinburgh, and Dublin Philosophical Magazine and Journal of Science*, *27*(182), pp.250-261.

[10] Allen, E. and Zalewski, W., 2009. *Form and forces: designing efficient, expressive structures*. John Wiley & Sons.

[11] Bow, R.H., 1873. *Economics of construction in relation to framed structures*. E. & FN Spon.

[12] Block, P., Ciblac, T. and Ochsendorf, J., 2006. Real-time limit analysis of vaulted masonry buildings. *Computers & structures*, *84*(29-30), pp.1841-1852.

[13] Block, P.P.C.V., 2005. *Equilibrium systems: Studies in masonry structure* (Master's thesis, Massachusetts Institute of Technology).

[14] Huerta, S., 2008. The analysis of masonry architecture: A historical approach. *Architectural Science Review*, *51*(4), pp.297-328.

[15] Roca, P., Cervera, M. and Gariup, G., 2010. Structural analysis of masonry historical constructions. Classical and advanced approaches. *Archives of computational methods in engineering*, *17*(3), pp.299-325.

[16] Heyman, J., 1997. *The stone skeleton: structural engineering of masonry architecture*. Cambridge University Press.

[17] Ochsendorf, J.A., 2002. *Collapse of masonry structures* (Doctoral dissertation, University of Cambridge).

[18] Wittmann, W., 1879. Zur Theorie der Gewölbe. *Zeitschrift für Bauwesen*, *29*, pp.61-74.

[19] O'Dwyer, D., 1999. Funicular analysis of masonry vaults. *Computers & Structures*, *73*(1-5), pp.187-197.

[20] Block, P. and Ochsendorf, J., 2007. Thrust network analysis: a new methodology for three-dimensional equilibrium. *Journal of the International Association for shell and spatial*

structures, *48*(3), pp.167-173.

[21] Rippmann, M., 2016. *Funicular Shell Design: Geometric approaches to form finding and fabrication of discrete funicular structures* (Doctoral dissertation, ETH Zurich).

[22] López López D., Veenendaal, D., Akbarzadeh, M. and Block, P., 2014, September. Prototype of an ultra-thin, concrete vaulted floor system. In *Proceedings of IASS Annual Symposia* (Vol. 2014, No. 15, pp. 1-8). International Association for Shell and Spatial Structures (IASS).

[23] Popescu, M., Rippmann, M., Liew, A., Reiter, L., Flatt, R.J., Van Mele, T. and Block, P., 2020, March. Structural design, digital fabrication and construction of the cable-net and knitted formwork of the KnitCandela concrete shell. In *Structures*. Elsevier.

[24] Van Mele, T., Méndez Echenagucia, T., Pigram, D., Liew, A. and Block, P., 2018. A prototype of a thin, textile-reinforced concrete shell built using a novel, ultra-lightweight, flexible formwork system. *DETAIL Struct*, *1*, pp.50-53.

[25] Panozzo, D., Block, P. and Sorkine-Hornung, O., 2013. Designing unreinforced masonry models. *ACM Transactions on Graphics (TOG)*, *32*(4), pp.1-12.

[26] Block, P. and Lachauer, L., 2014. Three-dimensional (3D) equilibrium analysis of gothic masonry vaults. *International Journal of Architectural Heritage*, *8*(3), pp.312-335.

[27] Block, P. and Lachauer, L., 2014. Three-dimensional funicular analysis of masonry vaults. *Mechanics Research Communications*, *56*, pp.53-60.

[28] Van Mele, T., Panozzo, D., Sorkine-Hornung, O. and Block, P. (2014). 'Best-fit thrust network analysis', in Adriaenssens, S., Block, P., Veenendaal, D. and Williams, C. eds. *Shell structures for architecture: form finding and optimization*. Oxon: Routledge, pp.157-170.

[29] Schek, H.J., 1974. The force density method for form finding and computation of general networks. *Computer methods in applied mechanics and engineering*, *3*(1), pp.115-134.

[30] Roca, P., López-Almansa, F., Miquel, J. and Hanganu, A., 2007. Limit analysis of reinforced masonry vaults. *Engineering Structures*, *29*(3), pp.431-439.

7. ANNEX

As mentioned in chapter 4 and 5, the numerical results and detailed analysis for the seven combinations of mesh types and load cases are presented in corresponding sections in this annex.

7.1. Mesh 1 + Load case 1

Form diagram 1.1 contains the basic square grid pattern.
Form diagram 1.2 and 1.3 have the same pattern as 1.1 does, but of higher densities, and 1.3 is the densest one.
Form diagram 1.4 has a quadrilateral grid pattern adapted from 1.1. Lines of grids are curved inwards, forming a series of arches.
Form diagram 1.5 and 1.6 follow the same pattern as that of 1.4 but of higher densities. Among them, 1.6 contains the highest density.
Form diagram 1.7, 1.8, 1.9, and 1.10 are all generated through superimposing additional patterns with 1.1. 1.7 has an additional arch pattern with arches collecting forces to the supports. 1.8 is similar to 1.7, but the curvatures of some arches are slightly different. A diagonal pattern is added for 1.9 with more paths to transfer loads to the edge arches. 1.10 has more paths to transfer forces directly to the supports.

1.1	1.2	1.3
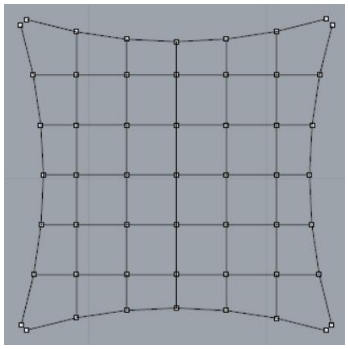	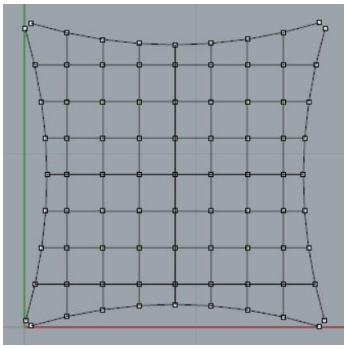	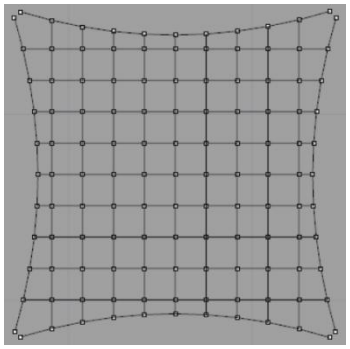
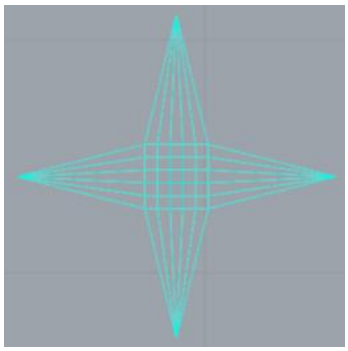	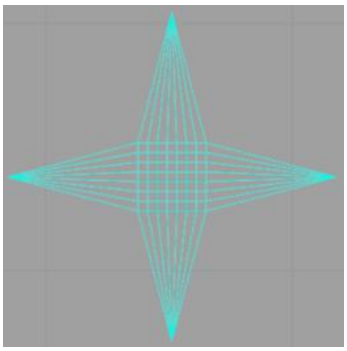	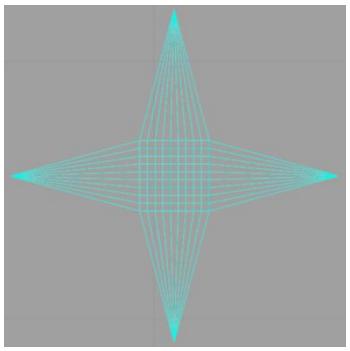
0.00035	0.00036	0.00036

1.4

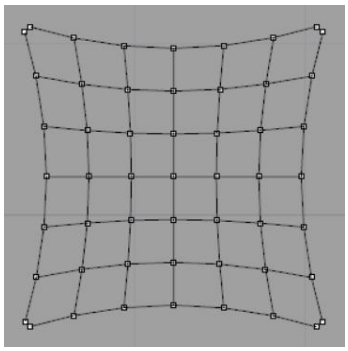

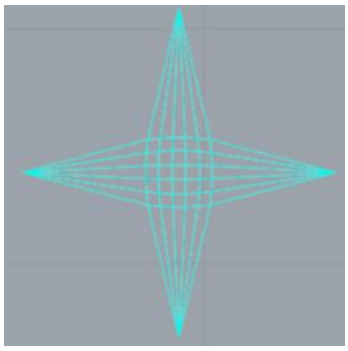

0.00035

1.5

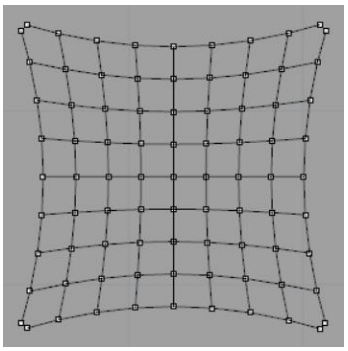

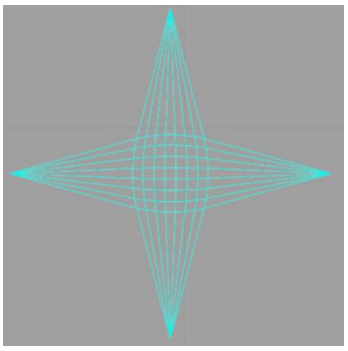

0.00034

1.6

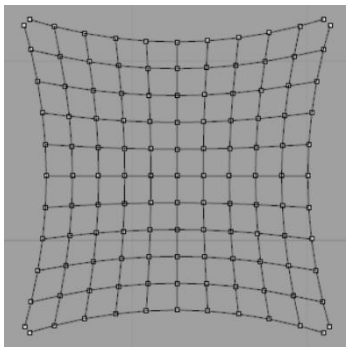

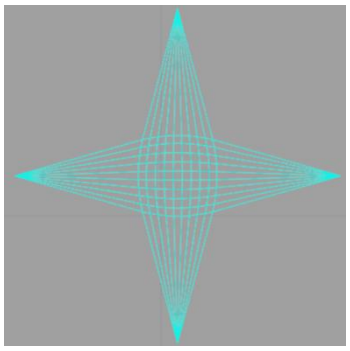

0.00035

1.7

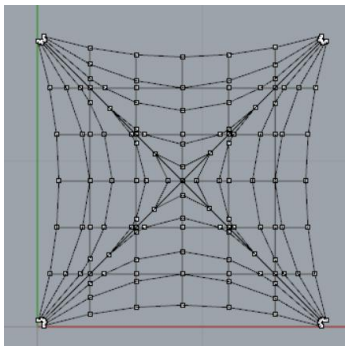

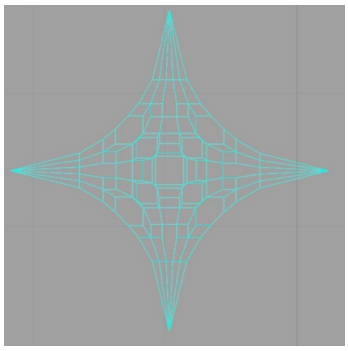

0

1.8

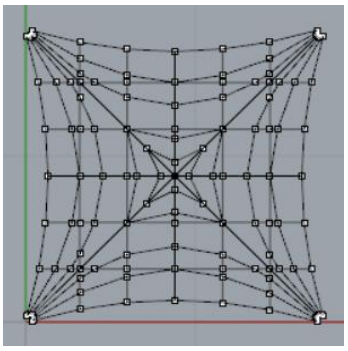

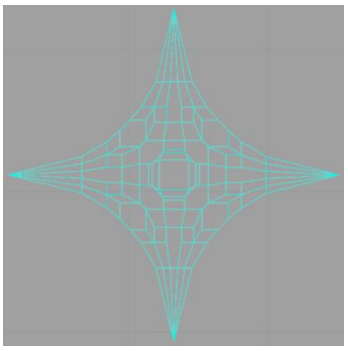

0.00065

1.9

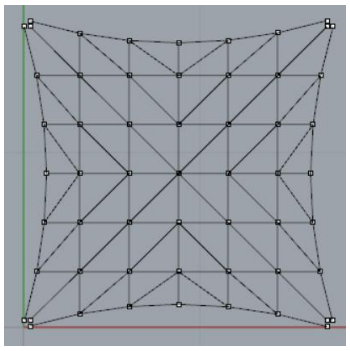

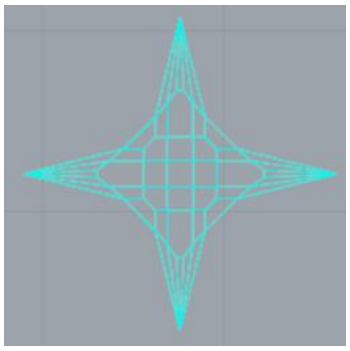

0.00040

1.10

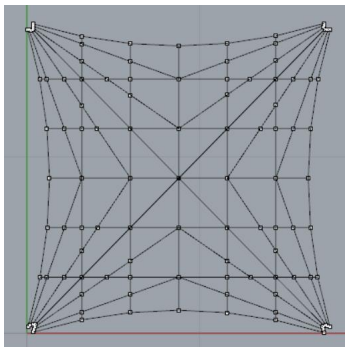

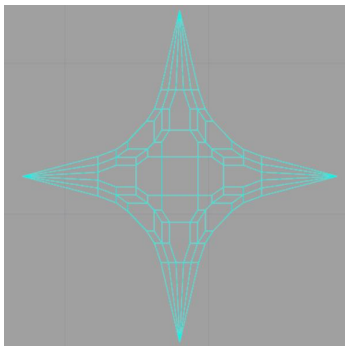

0.00055

Table A-1. Form diagrams (black lines), force diagrams (blue lines) and the minimal reinforcement amount for mesh 1 under load case 1

case	mesh	Load case	h/m	θ/°	t/m	A/cm^2
1.1	1	1	0.78	0	0.089	0.00035
1.2	1	1	0.77	0	0.089	0.00036
1.3	1	1	0.76	0	0.089	0.00036
1.4	1	1	0.72	0	0.089	0.00035
1.5	1	1	0.70	0	0.089	0.00034
1.6	1	1	0.70	0	0.089	0.00035
1.7	1	1	0.41	-	-	0
1.8	1	1	0.59	0	0.089	0.00065
1.9	1	1	0.61	0	0.089	0.00040
1.10	1	1	0.62	0	0.089	0.00055

Table A-2. Detailed results for mesh 1 under load case 1

Comparing 1.1, 1.2, and 1.3

These three form diagrams follow the same square grid pattern. Among them, 1.3 contains the densest mesh and 1.1 the loosest. The results suggest that 1.2 and 1.3 are the same and slightly better than 1.1.

Comparing 1.4, 1.5, and 1.6

The patterns of grids of these three form diagrams are the same, but the densities are different. 1.6 is the densest and 1.4 the loosest. 1.4 and 1.6 result in the same amount of reinforcement, and 1.5 requires less reinforcement than them.

Comparing 1.1 with 1.4, 1.2 with 1.5, and 1.3 with 1.6

Members of each pair have the same density, but different patterns. The results suggest that the latter one of each pair is better as they require less reinforcement, except for the first pair that 1.4 has the same result as 1.1.

It is observed that the results of the first six form diagrams (from 1.1 to 1.6) are all very close. The influence of the grid's density and pattern on the results are very slight under this load condition. It is hard to tell how the grid's density and pattern affect the results.

Comparing 1.1, 1.7, 1.8, 1.9 and 1.10

The last four form diagrams are all generated based on 1.1 with different additional patterns. According to the results, 1.7 seems to be an ideal pattern for this sail dome under self-weight as it requires no reinforcement at all. On the contrary, 1.8, though very similar to 1.7, requires the most reinforcement. Compared to 1.1, though 1.8, 1.9, and 1.10 provide more force paths than 1.1, their results are even worse.

1.7 is sophisticated because it provides more paths for the forces to be transferred to the supports. However, this reason cannot explain the case of 1.8, 1.9, and 1.10, as they all offer additional paths. Regarding this contradiction, three reasons are possible:

(1) 1.8, 1.9, and 1.10 may contain unfavorable force paths, which ruin the results.

(2) The force distributions of 1.8, 1.9, and 1.10 are not proper. As the force diagram can be adjusted as well (introduced in section 2.6), the current one may not be suitable.

(3) The assumptions in ELARM's method [2].

For the first one, it may account for the case of 1.9 and 1.10. However, for 1.8, which is very close to 1.7, unexpectedly obtains the worst result. It could be that these small differences are so critical that they influence a lot on the results, while the possibility is not high.

For the second one, it is possible but cannot satisfactorily explain for the case of 1.8 either. The force diagrams of 1.7 and 1.8 are all generated automatically, and they are similar. It makes not much sense that these small differences would lead to such a gap between the results.

For the third hypothesis, one of the main assumptions in the calculation process of ELARM3D is the method to calculate the assigned width. The details are listed below, an extract from the doctoral dissertation of López López [2].

"Figure 125 illustrates the process to obtain it, which, in order to avoid further discretization and to simplify calculations, seeks to find the tributary area of the edge and an average width to be applied at the mentioned specific points. The first step is to copy and transform the thrust network by vertically projecting each of its vertices to the shell's middle surface. For each edge of the new network, the centroid of its adjacent faces is found (only one face if the edge is at the boundaries). The areas of the triangles defined by the face's centroid and the edge's start and end points are computed. Afterwards, the addition of both areas is divided by the length of the edge. The described process to obtain the width, b, is valid for any kind of primal grid's force pattern and results in a conservative value.

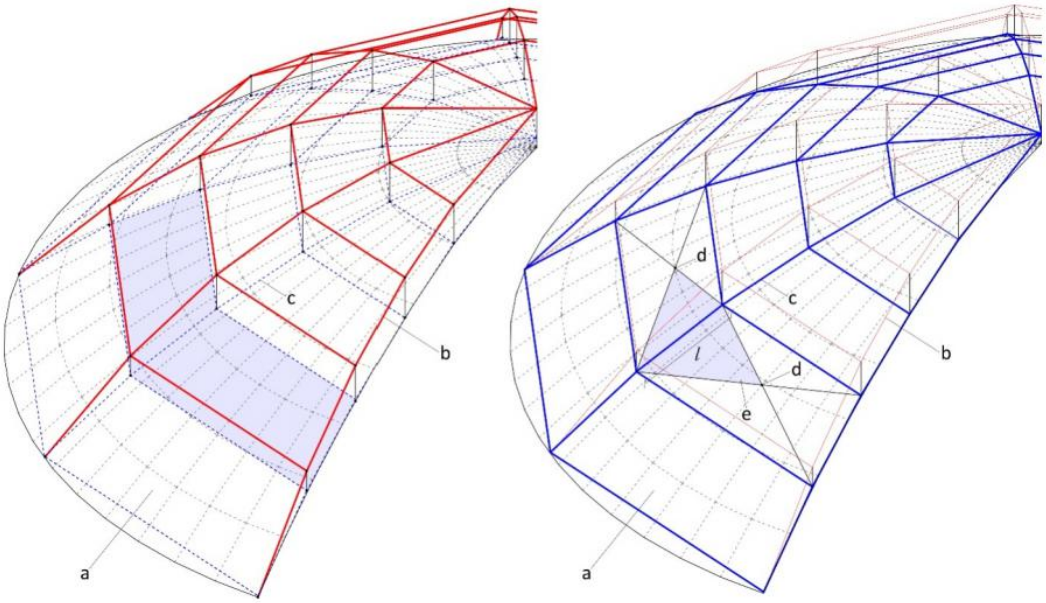

Figure 125. Figure illustrating in two steps the way to obtain the values to compute b, a) shell's middle surface, b) thrust network, c) transformed thrust network by projecting the vertices to the middle surface, d) centroids of the faces adjacent to the new network's analysed edge, e) area of the triangles defined by the faces' centroids and the edge's start and end points."

For 1.8, this method may cause the assigned widths of some edges to become very small, for example, the branches near the four corners and those in the middle. Branches are arranged very closely in these positions, so the tributary areas would be small, leading to small assigned widths. To compensate for the low value of the assigned width, the steel bar area should increase to ensure the safety of these branches.

For 1.7, it happens to be that A is zero. When defining the total amount of assigned steel, the assigned width is multiplied by A, while everything multiplied by zero is still zero. The method to calculate the assigned width will not have any influence on the result of 1.7. For 1.9 and 1.10, the added patterns also reduce the assigned widths of branches of the original pattern, so that the third reason in some way explains why the results of 1.9 and 1.10 are higher than that of 1.1.

However, the third reason can not explain the whole problem. To what extent it influences the results is still unknown.

In summary, all of these three reasons are possible, and they may work together, even with other unknown reasons to influence the results.

7.2. Mesh 1 + Load case 2

The position of the point load is shown in fig. A-1.

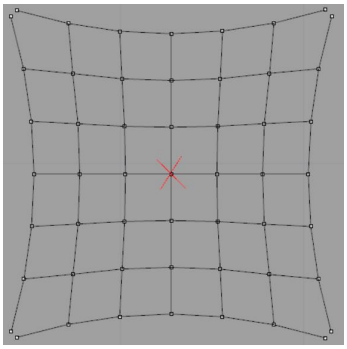

Fig. A-1. The position of the point load marked by the red cross

Form diagram 2.1 contains the basic square grid pattern.
Form diagram 2.2, 2.3, and 2.4 follow the same pattern as that of 2.1 but have higher densities.
Form diagram 2.5, 2.6, 2.7, 2.8, 2.9, and 2.10 are all generated by combining additional patterns with 2.1. 2.5, 2.6, 2.7, and 2.8 are the same as 1.10, 1.9, 1.7, and 1.8, respectively. 2.9 provides more paths from the midpoint directly to the supports. 2.10 is close to 2.9 but contains paths from the midpoint to the edge arches as well.
Form diagram 2.11, 2.12, and 2.13 are the same as 1.4, 1.5, and 1.6, respectively.
Form diagram 2.14 has additional paths from the midpoint to the supports based on 2.11.
Form diagram 2.15 is close to 2.11, but the curvatures of lines are larger, resulting in steeper internal arches than those of 2.11. These arches allow collecting forces to the edge arches.
Form diagram 2.16 and 2.17 follows the same pattern as 2.15 but of higher densities (more internal arches).
Form diagram 2.18 has additional force paths from the midpoint to the supports based on 2.15.

2.1 2.2 2.3

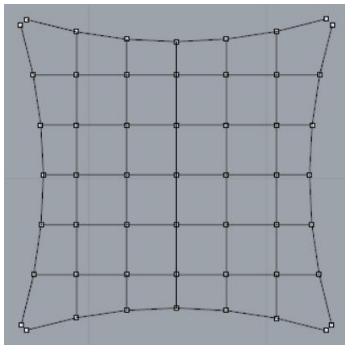
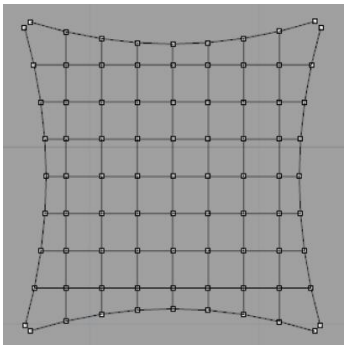
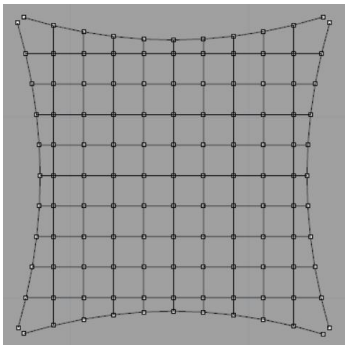
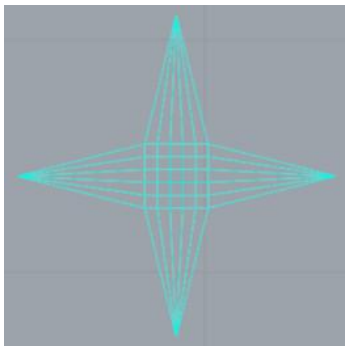
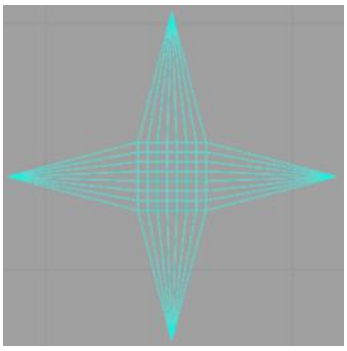
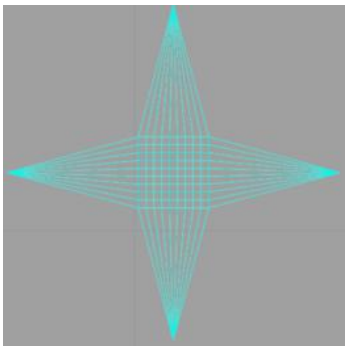

0.032 0.035 0.042

2.4 2.5 2.6

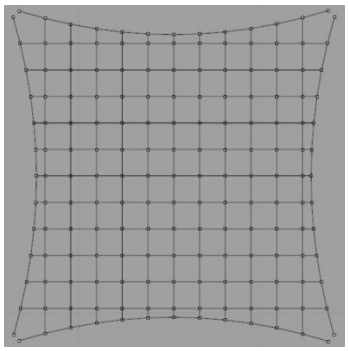
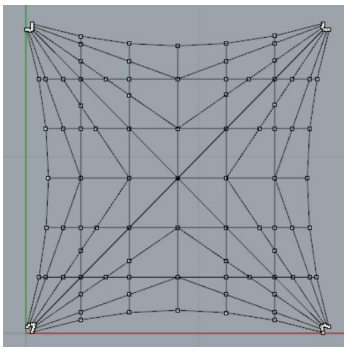
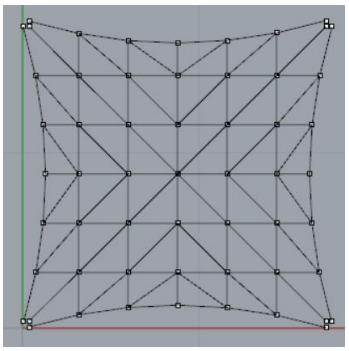
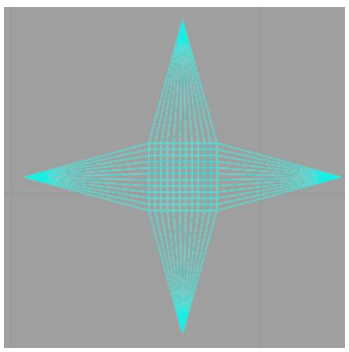
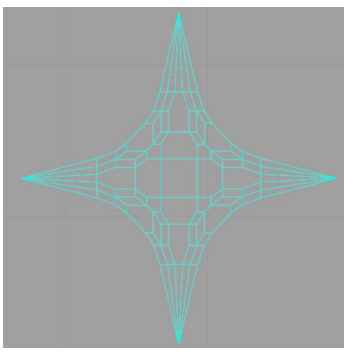
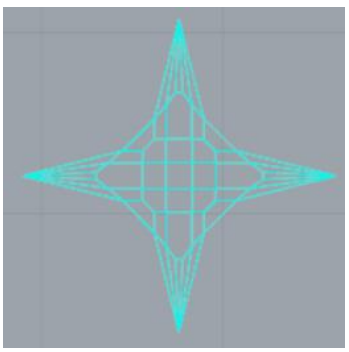

0.048 0.048 0.042

2.7 2.8 2.9

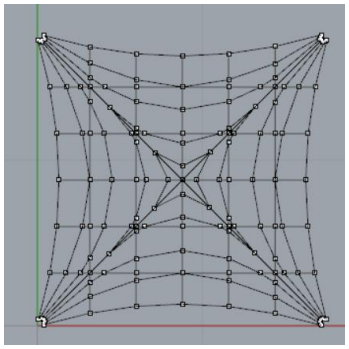
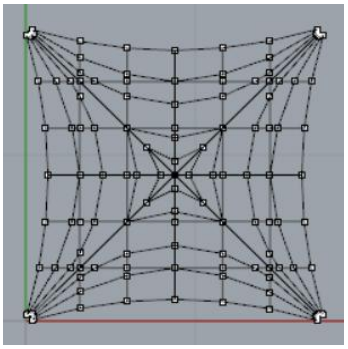
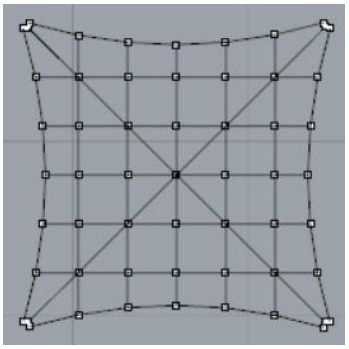
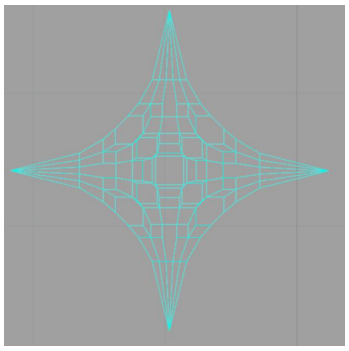
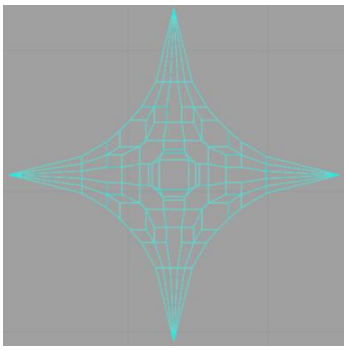
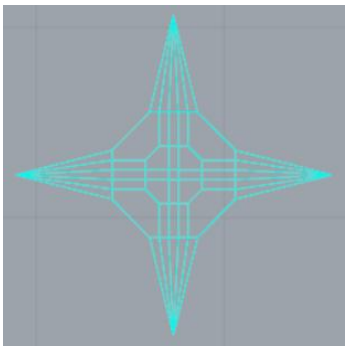

0.081 0.073 0.046

2.10 2.11 2.12

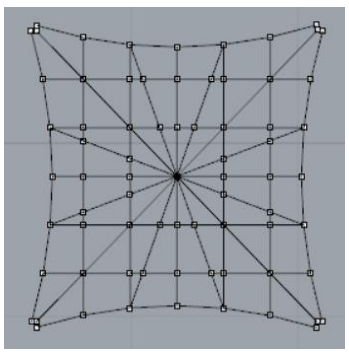
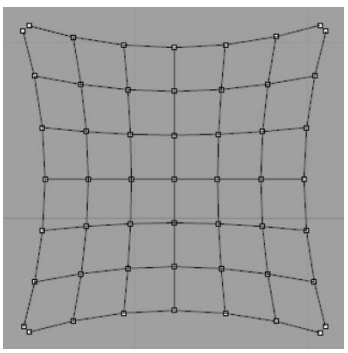
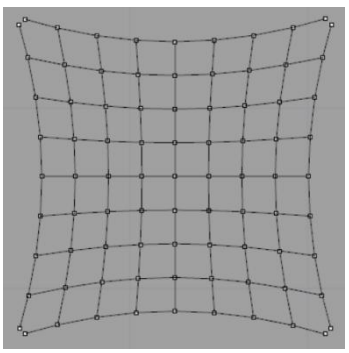
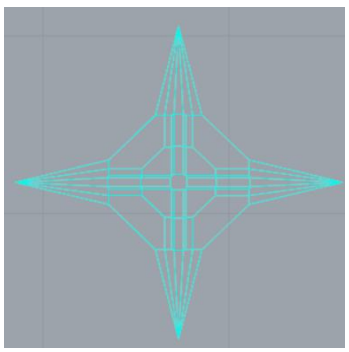
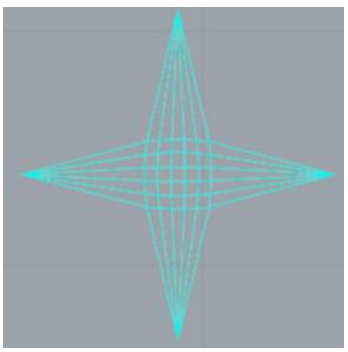
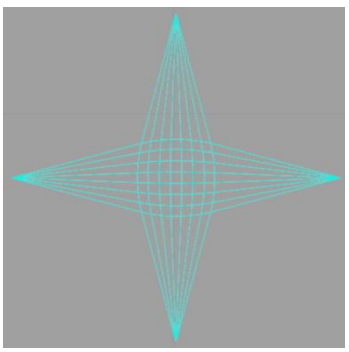

0.075 0.029 0.036

2.13 2.14 2.15

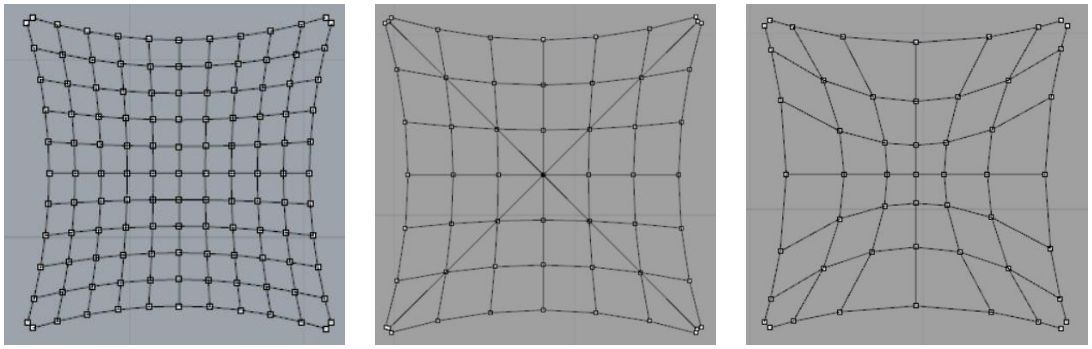

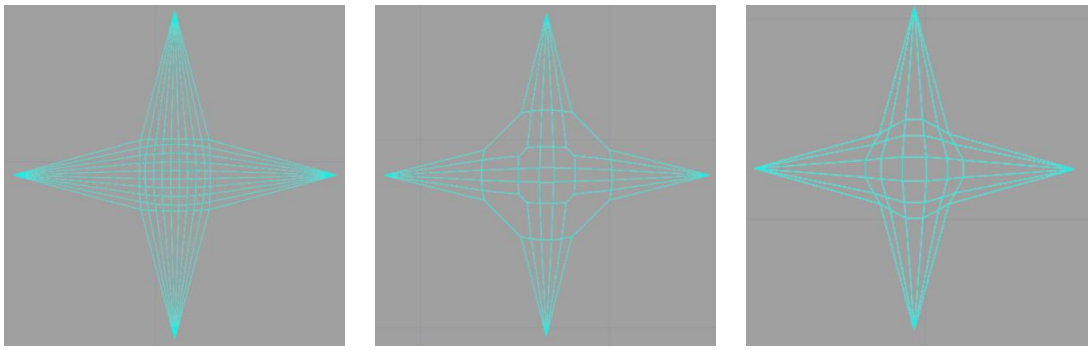

0.042 0.038 0.040

2.16 2.17 2.18

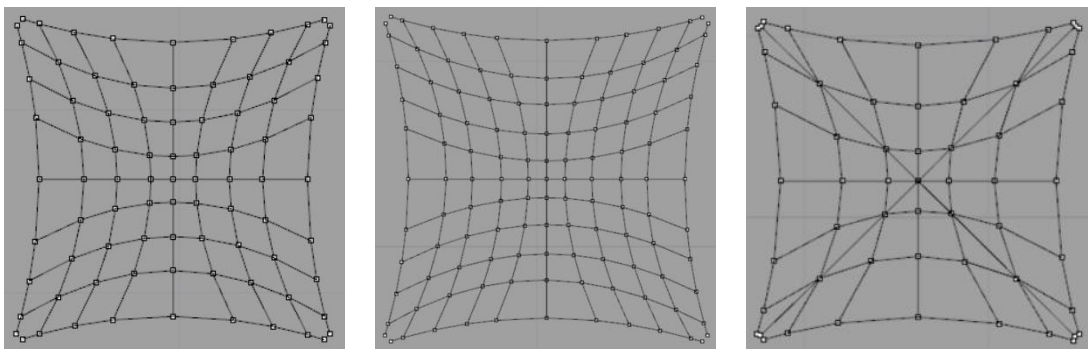

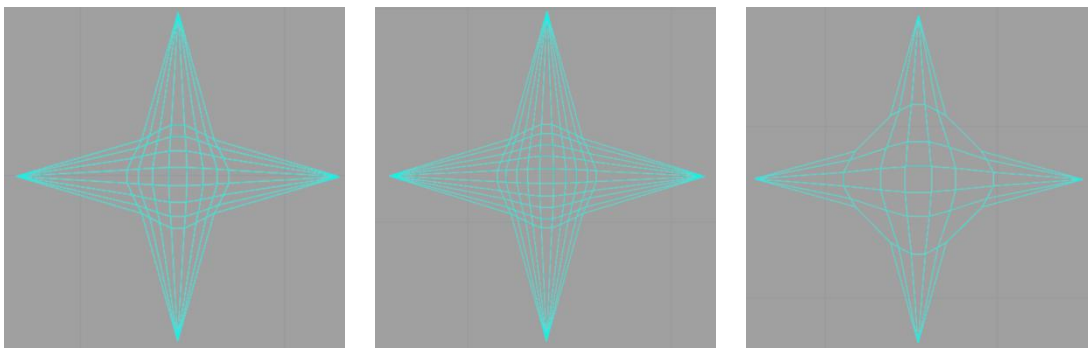

0.042 0.049 0.048

Table A-3. Form diagrams (black lines), force diagrams (blue lines) and the minimal reinforcement amount for mesh 1 under load case 2

case	mesh	Load case	h/m	θ/°	t/m	A/cm^2
2.1	1	2	3.33	0	0.089	0.032
2.2	1	2	3.70	0	0.089	0.035
2.3	1	2	3.95	0	0.089	0.042
2.4	1	2	4.20	0	0.089	0.048
2.5	1	2	2.08	0	0.089	0.048
2.6	1	2	2.26	0	0.089	0.042
2.7	1	2	2.50	0	0.089	0.071
2.8	1	2	2.33	0	0.089	0.073
2.9	1	2	4.43	0	0.089	0.046
2.10	1	2	3.55	0	0.089	0.075
2.11	1	2	2.90	0	0.089	0.029
2.12	1	2	3.20	0	0.089	0.036
2.13	1	2	3.36	0	0.089	0.042
2.14	1	2	3.30	0	0.089	0.038
2.15	1	2	2.05	0	0.089	0.040
2.16	1	2	2.18	0	0.089	0.042
2.17	1	2	2.40	0	0.089	0.049
2.18	1	2	0.90	0	0.048	0.048

Table A-4. Detailed results for mesh 1 under load case 2

Comparing 2.1, 2.2, 2.3 and 2.4

These four form diagrams have the same pattern of the grid but different densities. The results suggest that as the density increases, the required reinforcement amount is higher.

Comparing 2.11, 2.12 and 2.13

The patterns of these three form diagrams are the same, while the densities of grids are different. From the results, it is observed that a form diagram with denser grids requires more reinforcement.

Comparing 2.15, 2.16 and 2.17

Again, these three form diagrams have the same pattern of grids but different densities. The required reinforcement amount increases as the grids become denser.

These three groups of form diagrams are used to investigate the influence of the density on the required reinforcement amount. The force diagrams indicate that the force distributions in these form diagrams are all uniform, which is basically correct so that the influence of the force diagram can be neglected. However, adding density may influence the results from the other two aspects. It reduces the assigned width of each branch, and may influence the quality of the form diagram. Thus, it is hard to tell that whether adding density makes the form diagram more reasonable or not.

Anyway, according to the numerical results, for the current version of ELARM3D, the form diagram with a higher density would require more reinforcement.

Comparing 2.1, 2.11 with 2.15, 2.2, 2.12 with 2.16, and 2.3, 2.13 with 2.17

Members in each of these three groups have the same density but different grid patterns. According to the force diagrams, the first two patterns' force distributions are more uniform than the third one. For the assigned widths of branches, though the densities of members in each group are the same, the assigned widths are different due to the different arrangements of the branches. Thus, it cannot be known which pattern is more reasonable to transfer the internal forces. According to the numerical results, what can be known is that the third grid pattern always performs worse than the first two, and for the first two, the results are similar, and which one performs better depends on the density of the grids.

Comparing 2.1, 2.5, 2.6, 2.7, 2.8, 2.9, and 2.10

2.5, 2.6, 2.7, 2.8, 2.9, and 2.10 combine additional patterns with 2.1, which is the most basic pattern. Results show that all of these form diagrams with additional patterns require more reinforcement than the basic grid pattern. Such a result seems to be contrary to the intuition that allowing more reasonable force paths should lead to a more accurate form diagram with a better result, i.e., less reinforcement. As mentioned above, this is because the obtained results do not solely correspond to the qualities of the form diagrams. They are also influenced by the force diagram and the calculation process of ELARM3D.

It is not apparent whether the additional patterns of 2.5, 2.6, 2.7, and 2.8 are reasonable or not due to their complex geometries. However, for 2.9, it merely adds force paths directly from the location, where the point load is applied, to the supports. This is considered reasonable according to general intuition, but its result is still worse than that of 2.1.

The reason becomes clear after checking the force distributions in form diagram 2.9. ELARM3D allows checking axial forces in each branch. According to the data, the axial forces in the blue branches (fig. A-2) are around 0.090kN and those in the red branches (fig. A-2) are around 0.002kN. The ratio between them is about 45 to 1. Though the best force distribution is unknown due to its indeterminacy, this one is unreasonable. This is because the additional paths are built to attract forces to the support, while according to the data, the allocated forces in this path is extremely low. Besides, the additional branches even reduce the tributary areas of original branches, leading to smaller assigned widths. As a result, the steel bar area should be increased to compensate for the reduction of the assigned width so that the result of 2.9 is larger than that of 2.1.

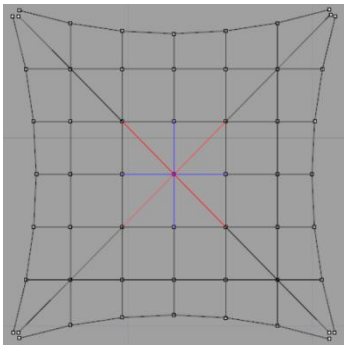

Fig. A-2. For 2.9, axial forces in the red branches being 45 times of those in the blue branches

In summary, for all these form diagrams with additional patterns, it is impossible to know whether these additional patterns are favorable or not from the statics. From the numerical results perspective, the basic grid pattern without any additional force paths achieves the best result, i.e., the least amount of reinforcement.

Comparing 2.11 with 2.14 and 2.15 with 2.18

These two pairs are used to investigate the influence of a specific additional pattern on the reinforcement amount for different grid patterns. Numerical results indicate that the one with additional paths presents worse results. To know the reasons, the force distributions of the form diagrams must be checked.

For 2.14, the axial forces in those blue branches (fig. A-3) are around 0.074kN, and the axial forces in those red branches (fig. A-3) are around 0.007kN, about one-tenth of those in the blue branches.

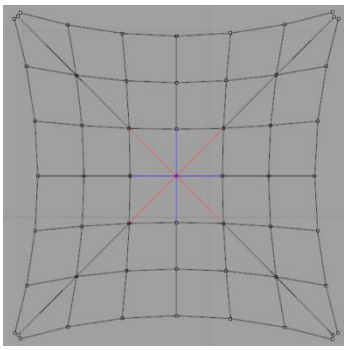

Fig. A-3. For 2.14, axial forces in the red branches being around 10 times of those in the blue branches

For 2.18, the axial forces in those blue branches (fig. A-4) are around 0.279kN, and the axial forces in those red branches (fig. A-4) are around 0.010kN, about one twenty-eighth of those in the blue branches.

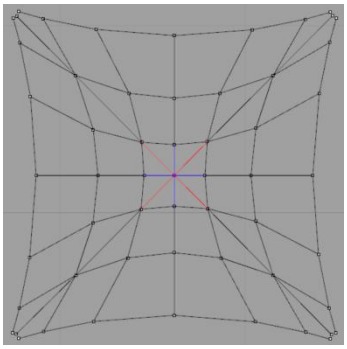

Fig. A-4. For 2.18, axial forces in the red branches being around 28 times of those in the blue branches

For 2.14 and 2.18, the additional branches do not attract enough force but take up the branches of the original branches' tributary area. In this way, the required reinforcement of these two become more extensive than the original patterns.

7.3. Mesh 1 + Load case 3

The position of the point load is shown in fig. A-5.

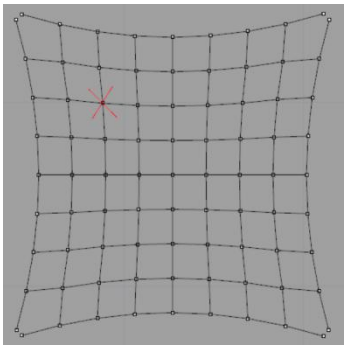

Fig. A-5. The position of the point load marked by the red cross

Form diagram 3.1 is the same as 1.5.

Form diagram 3.2, 3.3, 3.4, 3.5, and 3.6 are generated based on 3.1. 3.2 are partially triangulated to provide more paths from the load point to the nearby support and edge arches. 3.3 are triangulated providing more paths from the load point to all supports and edge arches. 3.4 offers additional paths from the load point directly to all supports. 3.5 add more force paths directly to the nearby edge arches and support. 3.6 just contains one more path from the load point directly to the nearest support.

3.1 3.2 3.3

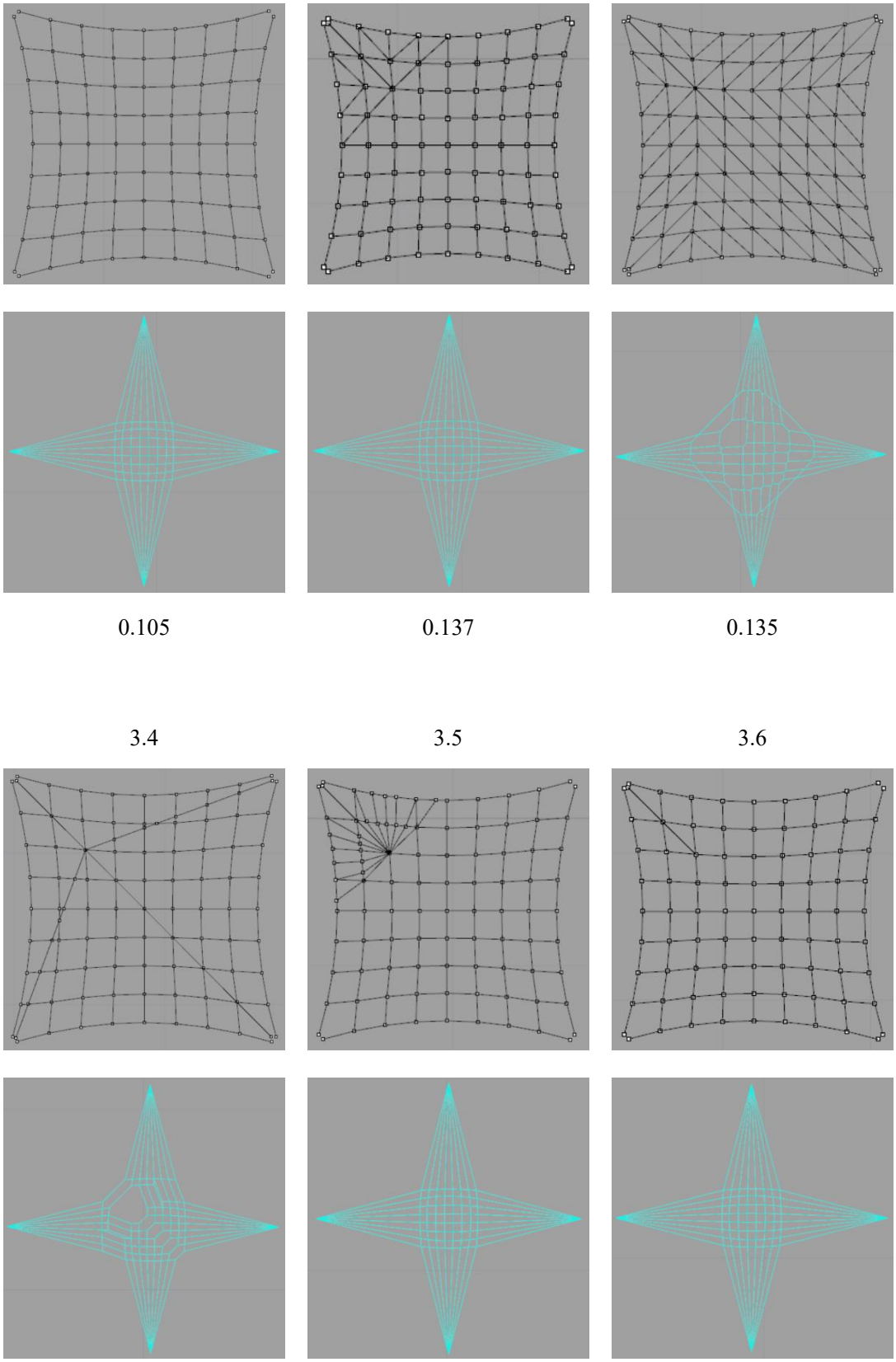

0.105	0.137	0.135
3.4	3.5	3.6
0.157	0.298	0.116

Table A-5. Form diagrams (black lines), force diagrams (blue lines) and the minimal reinforcement amount for mesh 1 under load case 3

case	mesh	Load case	h/m	θ/°	t/m	A/cm^2
3.1	1	3	2.61	0	0.049	0.105
3.2	1	3	2.91	0	0.061	0.137
3.3	1	3	2.14	0	0.060	0.135
3.4	1	3	1.48	0	0.069	0.157
3.5	1	3	1.15	0	0.041	0.298
3.6	1	3	2.70	0	0.054	0.116

Table A-6. Detailed results for mesh 1 under load case 3

Form diagram 3.2, 3.3, 3.4, 3.5, and 3.6 provide additional force paths based on 3.1. This section is to investigate the influence of these additional patterns on the reinforcement amount. According to the result, form diagrams with additional patterns all require more reinforcement than 3.1, the most basic one. As mentioned above, three different factors are influencing the final results. The force distribution of these form diagrams must be checked. It can be observed that the force diagrams of 3.1, 3.2, 3.5, and 3.6 are almost the same, which means that corresponding branches of the added patterns have almost zero lengths, indicating that the assigned forces on those additional branches are almost zero. It can be further checked through the data in ELARM3D. Take form diagram 3.6 as an example. The axial forces of the blue branches (fig. A-6) are around 0.201kN, while for the red one (fig. A-6), the axial force is 0.001kN, which is far smaller than the blue ones. This is unreasonable because the initial intention of adding the red branch is to transfer forces directly to the support. Besides, it also reduces the tributary areas of those blue branches. As a result, the required reinforcement amount turns out to be larger than that of 3.1.

In summary, as mentioned above, it is impossible to identify the rationality of the added force paths according to the numerical results, as the results are influenced by three factors together. What can be indicated from the results is that, in this section, the form diagram with no additional force paths requires the least reinforcement amount.

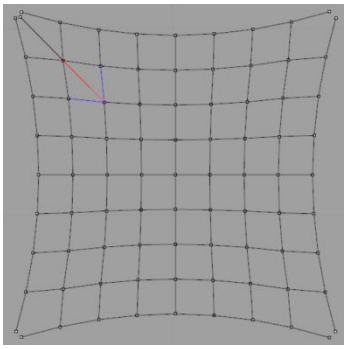

Fig. A-6. For 3.6, axial forces in the red branches being around 28 times of those in the blue branches

7.4. Mesh 2 + Load case 1

For a sail dome of a higher height-span ratio than mesh 1, under self-weight, this section investigates the influence of the grid pattern on the required reinforcement amount.

Form diagram 4.1 and 4.2 are the same as 1.1 and 1.4 respectively.

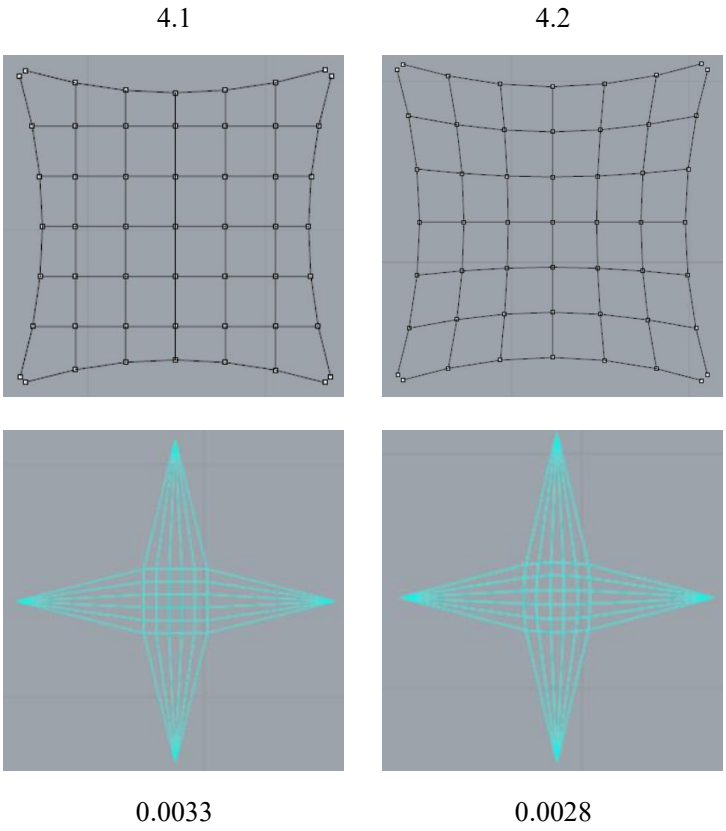

Table A-7. Form diagrams (black lines), force diagrams (blue lines) and the minimal reinforcement amount for mesh 2 under load case 1

case	mesh	Load case	h/m	θ/°	t/m	A/cm^2
4.1	2	1	2.45	0	0.029	0.0033
4.2	2	1	2.41	0	0.033	0.0028

Table A-8. Detailed results for mesh 2 under load case 1

Comparing 4.1 and 4.2,
The distributions of forces are uniform according to the force diagrams, which is acceptable. Though the densities of these two form diagrams are the same, the assigned widths are unlike due to the different geometries of the form diagrams. Thus, as already mentioned in previous sections,

the numerical results cannot identify which grid pattern provide more appropriate force paths. What can be known from the results is that the second grid pattern would require less reinforcement for this sail dome under self-weight for the current version of ELARM.

7.5. Mesh 2 + Load case 2

For the same sail dome as that in the previous section, but under the condition of a point loading applied at the midpoint of the sail dome, this section aims to investigate the influence of the grid pattern on the required reinforcement amount.

The position of the point load is shown in fig. A-7.

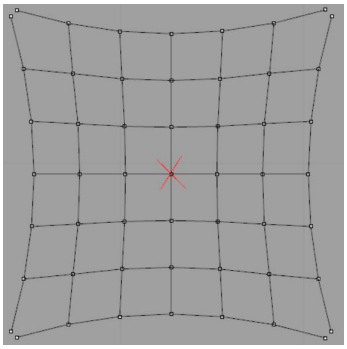

Fig. A-7. The position of the point load marked by the red cross

Form diagram 5.1 and 5.2 are the same as 1.1 and 1.4 respectively.

5.1 5.2

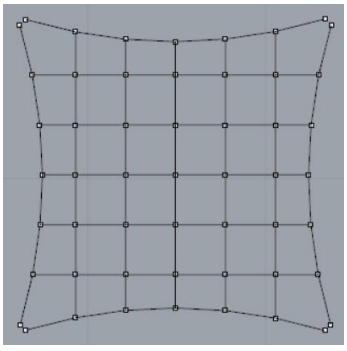

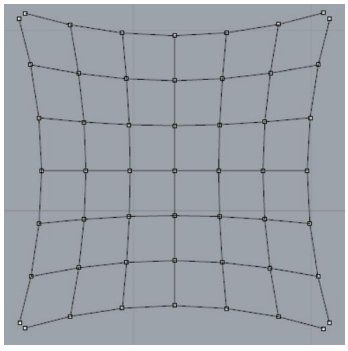

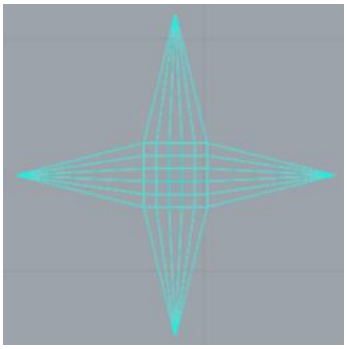

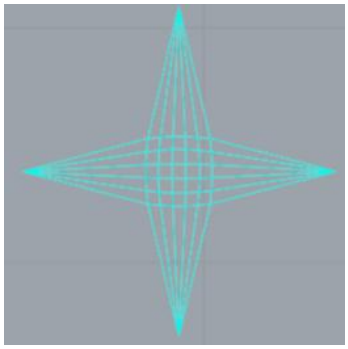

0.124 0.092

Table A-9. Form diagrams (black lines), force diagrams (blue lines) and the minimal reinforcement amount for mesh 2 under load case 2

case	mesh	Load case	h/m	θ/°	t/m	A/cm^2
1	2	2	4.64	0	0.027	0.124
2	2	2	4.50	0	0.039	0.092

Table A-10. Detailed results for mesh 2 under load case 2

Comparing 5.1 and 5.2,
The densities of these two form diagrams are the same, so that the assigned widths are close. The distributions of forces are both uniform according to the force diagrams, which is basically correct. Thus, the results reflect the quality of the pattern of the grid. Based on the result, it can be concluded that for this sail dome under a point load applied at the midpoint, the second grid pattern is a better choice.

7.6. Mesh 3 + Load case 2

This section is to explore the influence of form diagrams on the required reinforcement amount for a semi-spherical dome under self-weight.

The position of the point load is shown in fig. A-8.

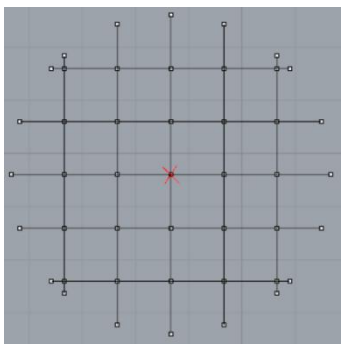

Fig. A-8. The position of the point load marked by the red cross

Form diagram 6.1 has a basic square grid pattern.

Form diagram 6.2 has the same pattern as that of 6.1, but a denser one.

Form diagram 6.3 and 6.4 are generated based on 6.1 and 6.2, respectively, containing more paths to the support.

Form diagram 6.5 is close to 6.1, but the lines are curved outward.

Form diagram 6.6 has a similar but denser pattern than 6.5.

Form diagram 6.7 and 6.8 are generated based on 6.5 and 6.6, respectively, containing more paths to the support.

Form diagram 6.9 is similar to 6.1, but the lines are curved inward, forming several internal arches.

Form diagram 6.10 has a similar but denser pattern than 6.9.

Form diagram 6.11 and 6.12 are generated based on 6.9 and 6.10, respectively, containing more paths to the support.

Form diagram 6.13 provides paths from the midpoint to the surrounding support, and the internal circles allow the development of circumferential forces.

Based on 6.13, 6.14 adds more force paths in the circumferential direction, 6.15 adds more force paths in the radial direction, and 6.16 increases the densities in both directions.

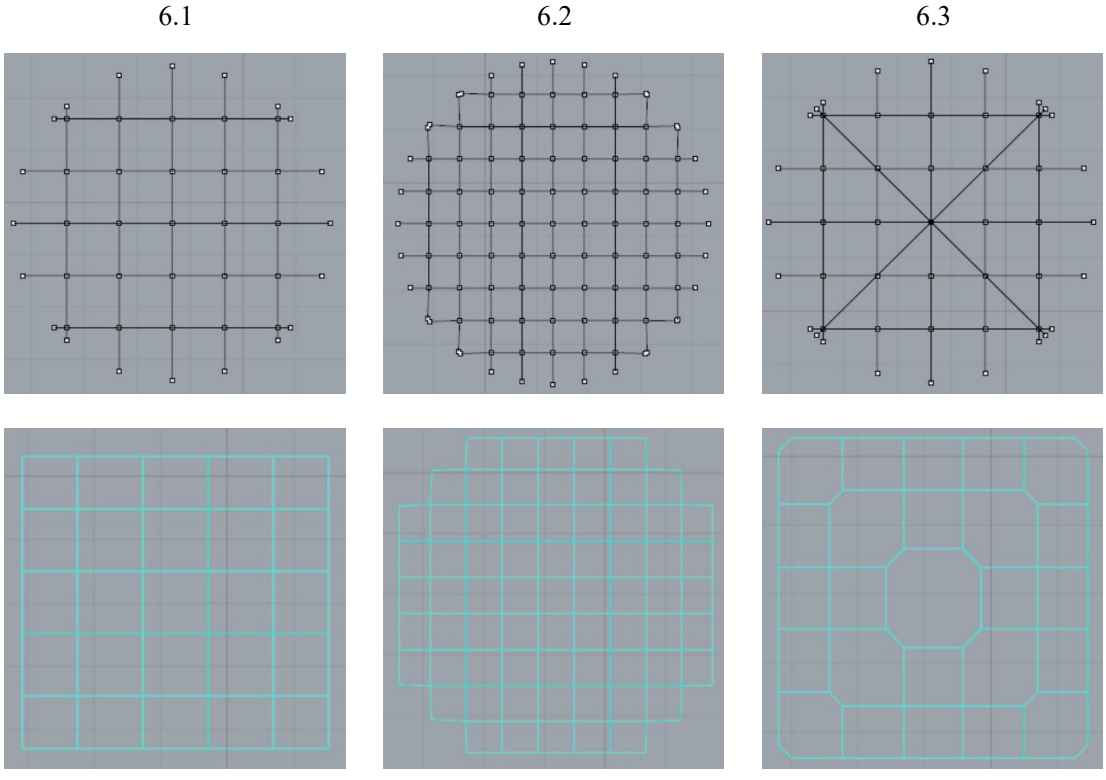

6.4

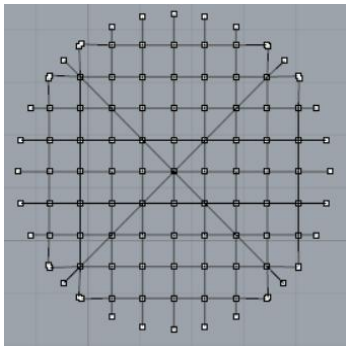

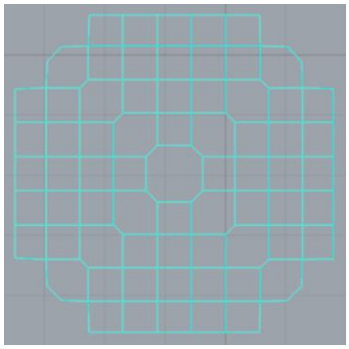

0.019

6.5

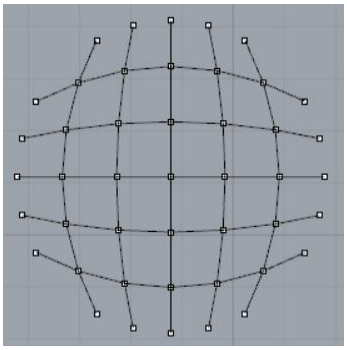

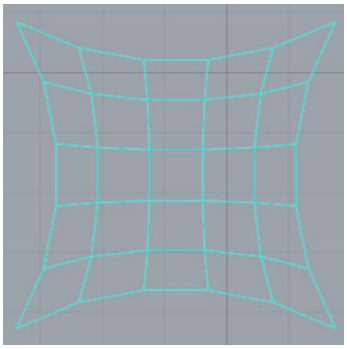

0.025

6.6

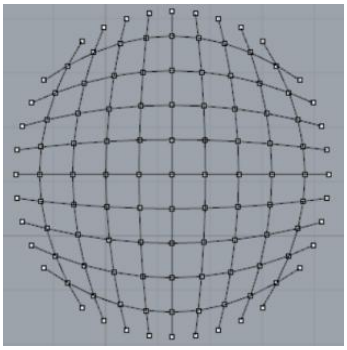

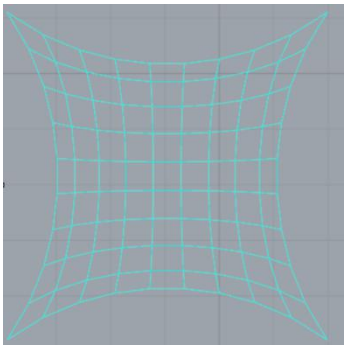

0.030

6.7

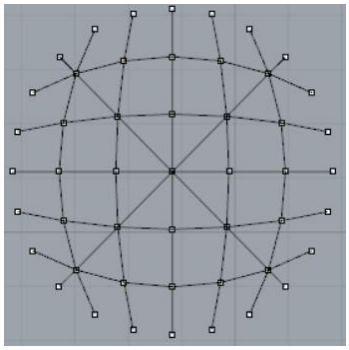

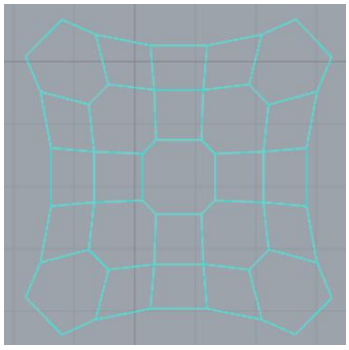

0.021

6.8

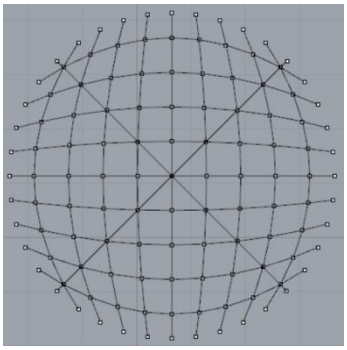

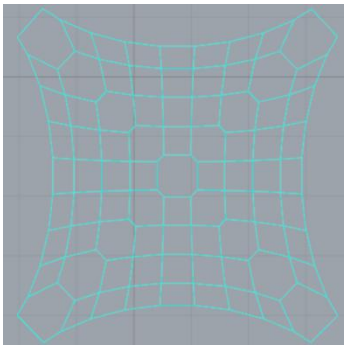

0.027

6.9

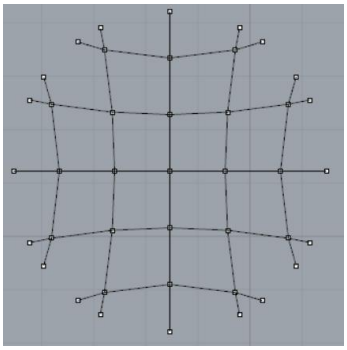

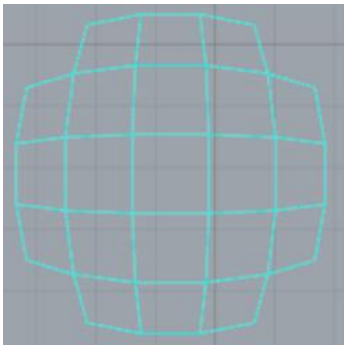

0.013

6.10

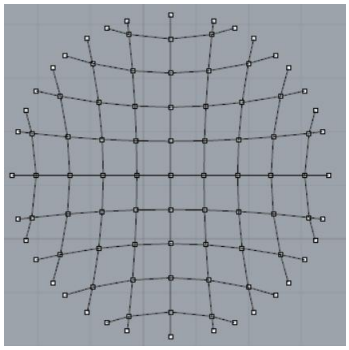

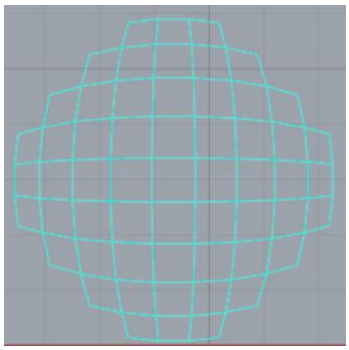

0.019

6.11

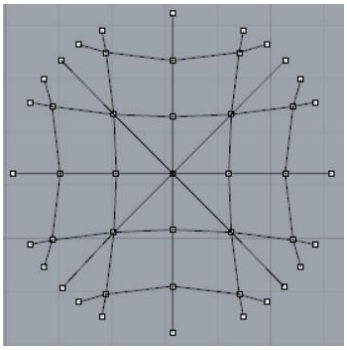

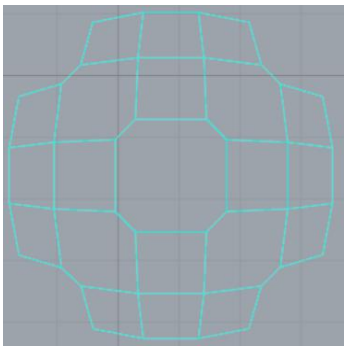

0.010

6.12

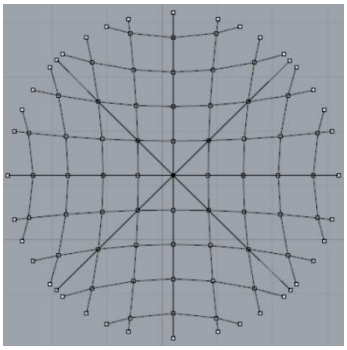

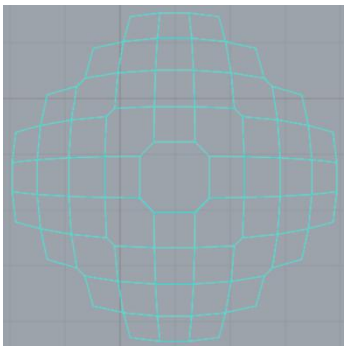

0.015

6.13

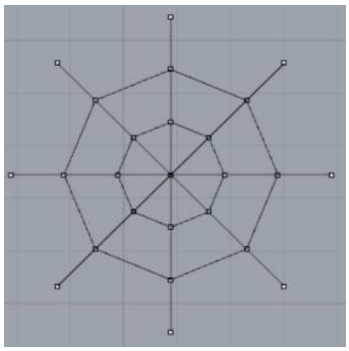

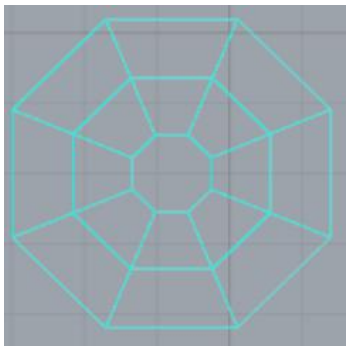

0.018

6.14

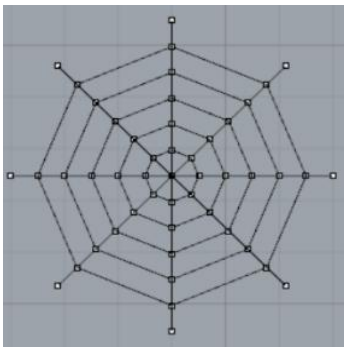

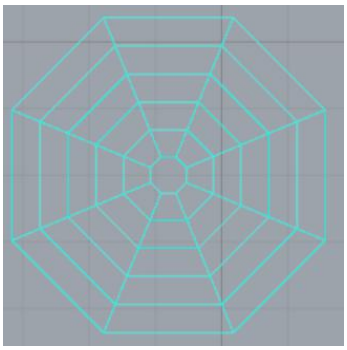

0.027

6.15

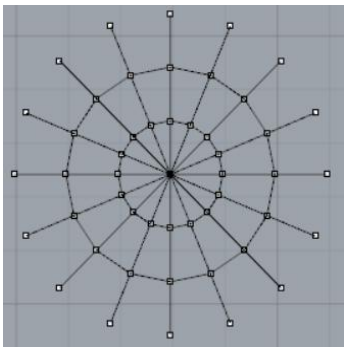

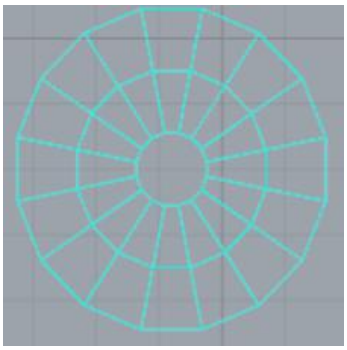

0.018

6.16

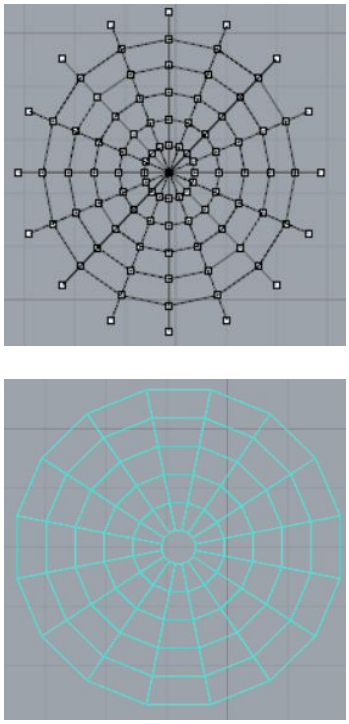

0.026

Table A-11. Form diagrams (black lines), force diagrams (blue lines) and the minimal reinforcement amount for mesh 3 under load case 2

case	mesh	Load case	h/m	θ/°	t/m	A/cm^2
6.1	3	2	3.80	0	0.001	0.018
6.2	3	2	3.76	0	0.001	0.023
6.3	3	2	3.78	0	0.001	0.015
6.4	3	2	3.64	0	0.001	0.019
6.5	3	2	3.90	0	0.001	0.025
6.6	3	2	3.80	0	0.001	0.030
6.7	3	2	3.89	0	0.001	0.021
6.8	3	2	3.70	0	0.001	**0.027**
6.9	3	2	3.84	0	0.001	0.013
6.10	3	2	3.72	0	0.001	0.019
6.11	3	2	3.74	0	0.001	0.010
6.12	3	2	3.59	0	0.001	0.015
6.13	3	2	3.95	0	0.001	0.018
6.14	3	2	3.75	0	0.001	0.027
6.15	3	2	4.00	0	0.001	0.018
6.16	3	2	3.80	0	0.001	0.026

Table A-12. Detailed results for mesh 3 under load case 2

Comparing 6.1 with 6.2, 6.5 with 6.6, and 6.9 with 6.10

These three pairs of form diagrams are used to investigate the influence of the density on the required reinforcement amount. The force diagrams indicate that the force distributions in these form diagrams are all uniform, which is basically correct so that the influence of the force diagram can be neglected. However, adding density reduce the assigned width of each branch, so it is hard to tell which factor result in such results, the quality of the form diagram, or the method to calculate the assigned width. Anyway, for the current version of ELARM3D, the results suggest that the form diagram with a higher density would require more reinforcement.

Comparing 6.13, 6,14, 6.15 and 6.16

This is to investigate the influence of densities of branches in the radial direction and the circumferential direction for form diagrams of a special type. As mention above, it is unknown whether the force distributions are the most appropriate and whether the assumption to calculate the assigned width in ELARM3D is proper, the numerical results indicate that adding the density of ranches in the radial direction would lead to a worse result, while the density of the branches in the circumferential direction has little influence on the reinforcement amount.

Comparing 6.1, 6.5 and 6.9

The densities of these three form diagrams are close, so that the assigned widths will not have a large influence on the results. The distributions of forces are both uniform according to the force diagrams, which is basically correct. Thus, the results basically reflect the quality of the grid pattern. Based on the results, it can be concluded that for this semi-spherical dome under self-weight, the third grid pattern is a good choice, as it forms a series of arches to collect forces to the supports.

Comparing 6.2, 6.6 and 6.10

This is to investigate whether the third gird pattern performs the best when the density becomes higher. As mentioned above, the influence of the assigned width and force diagram basically can be excluded. The results only reflect on the quality of the grid pattern. The results present the same rule as above that the third pattern is the more appropriate one among these three different grid patterns. It would be better to generate the form diagram with concave lies forming arches to collect forces to the supports.

Comparing 6.1 with 6.3, 6.2 with 6.4, 6.5 with 6.7, 6.6 with 6.8, 6.9 with 6.11, and 6.10 with 6.12

All these six pairs are used to investigate the influence of additional force paths on the required reinforcement amount. All the results show that the one with additional force paths achieves better results. Before the conclusion, the force distributions should be checked.

For 6.3, as shown in fig. A-9, the axial forces in the red branches are around 0.178kN and are 0.315kN for those blue branches. It means that the diagonal paths do help to transfer forces to the supports. Though it is unknown whether this is the best force distribution or not, basically such distribution is acceptable. The cases of 6.4, 6.7, 6.8, 6.11, and 6.12 are shown in fig. A-10 - A-14. The axial forces in the red branches are all at the same order of magnitude as the axial forces in the blue branches. Basically, the force distributions are acceptable, though may not be the best.

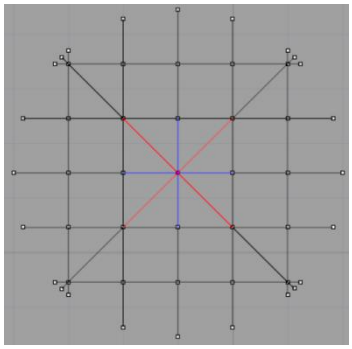

Fig. A-9. For 6.3, axial forces in the red branches are 0.178kN, and in the blue branches are 0.315kN

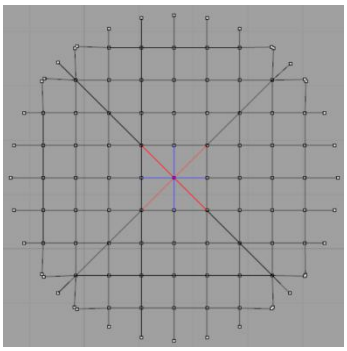

Fig. A-10. For 6.4, axial forces in the red branches are 0.110kN, and in the blue branches are 0.220kN

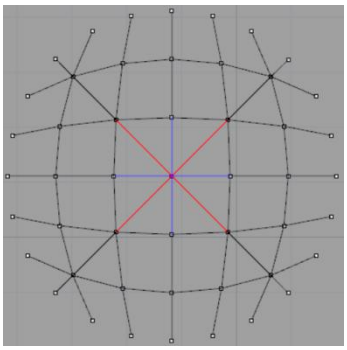

Fig. A-11. For 6.7, axial forces in the red branches are 0.139kN, and in the blue branches are 0.304kN

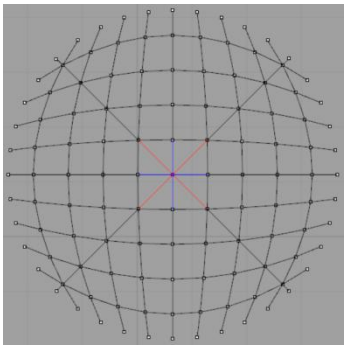

Fig. A-12. For 6.8, axial forces in the red branches are 0.083kN, and in the blue branches are 0.231kN

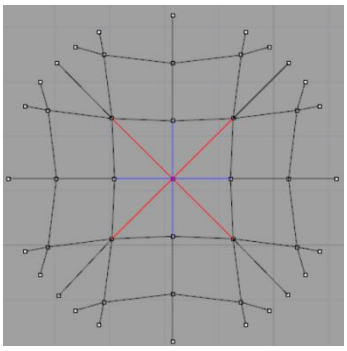

Fig. A-13. For 6.11, axial forces in the red branches are 0.152kN, and in the blue branches are 0.355kN

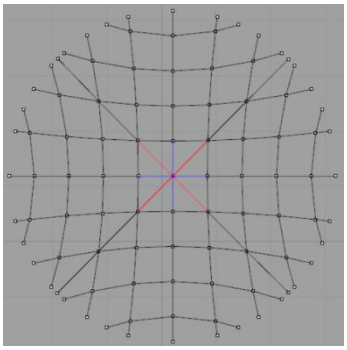

Fig. A-14. For 6.12, axial forces in the red branches are 0.124kN, and in the blue branches are 0.246kN

Though the additional paths take up some tributary areas of the original branches, they share a certain amount of forces as well. As a result, the required reinforcement amount is reduced. This indicates the effectiveness of the additional force paths.

7.7. Mesh 4 + Load case 2

In this section, the thickness of the vault is doubled to be 0.180 m. The position of the point load is shown in fig. A-15.

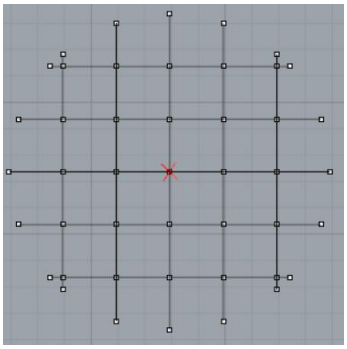

Fig. A-15. The position of the point load marked by the red cross

Form diagram 7.1, 7.2 and 7.3 are the same as 6.1, 6.5 and 6.9 respectively.

7.1	7.2	7.3
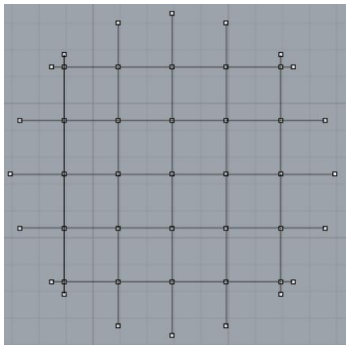	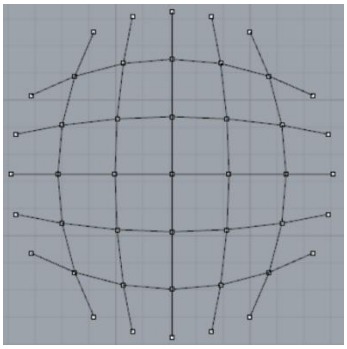	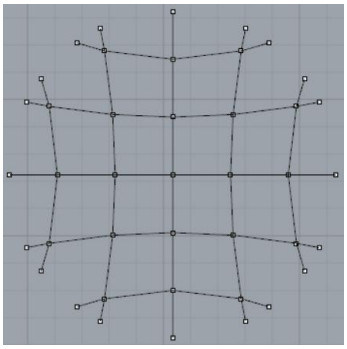
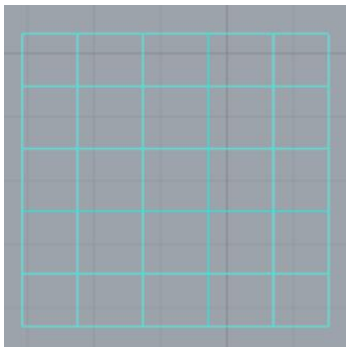	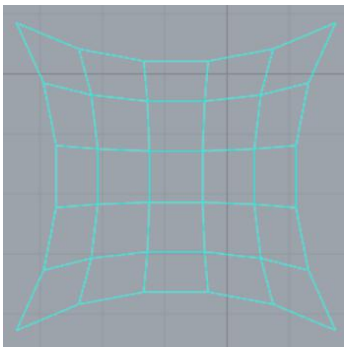	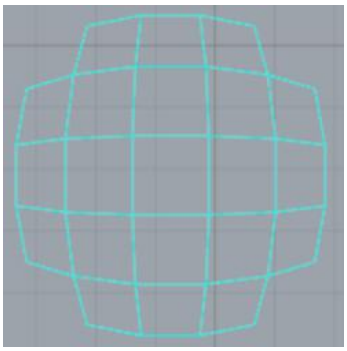
0.027	0.040	0.018

Table A-13. Form diagrams (black lines), force diagrams (blue lines) and the minimal reinforcement amount for mesh 4 under load case 2

case	mesh	Load case	h/m	θ/°	t/m	A/cm^2
7.1	4	2	6.7	0	0.001	0.027
7.2	4	2	6.8	0	0.001	0.040
7.3	4	2	6.7	0	0.001	0.018

Table A-14. Detailed results for mesh 4 under load case 2

This section is used to investigate the influence of grid pattern on the reinforcement amount, under the situation of a different vault. The results present the same rule as that obtained with mesh 3 that, the third pattern achieves the best result, and the second one the worst.